Manuscript prepared for J. Name
with version 2015/09/17 7.94 Copernicus papers of the LaTeX class copernicus.cls.
Date: 2 May 2017

Response to Editor

'Open-source sea ice drift algorithm for Sentinel-1 SAR imagery using a combination of feature-tracking and pattern-matching'

Stefan Muckenhuber and Stein Sandven

Nansen Environmental and Remote Sensing Center (NERSC), Thormøhlensgate 47,
5006 Bergen, Norway

Correspondence to: S. Muckenhuber (stefan.muckenhuber@nersc.no)

Dear Professor Lars Kaleschke,

Thank you very much for helping us improving our paper.

Please find here the **answers** to your comments:

1 Comment from the editor

The manuscript requires further major revisions before it can be accepted. In addition to the comments raised by the referees I'd like to add that some figures need to be improved, e.g. the black vectors in Fig. 3 are largely overlapping and Figure 8 looks really strange.

We changed several parts of the manuscript, adjusted the algorithm, recomputed the parameter evaluation and validation with the new algorithm version and included an evaluation of the algorithm performance for HH polarisation.
We changed the vector spacing in Figure 3 to improve the visibility of the individual vectors and replaced the vectors in Figure 8 by dots to get a better impression of the buoy data locations. In addition, we included information about the retrieved cross-correlation values in Figure 3.
We hope that the new version will meet the high standards of The Cryosphere.

Please find attached the corrected manuscript with changes marked in blue and red.

Thanks again for your comments. We are looking forward to your reply!

Best regards,
S. Muckenhuber and S. Sandven

Manuscript prepared for J. Name
with version 2015/09/17 7.94 Copernicus papers of the LaTeX class copernicus.cls.
Date: 2 May 2017

Response to Referee # 1

'Open-source sea ice drift algorithm for Sentinel-1 SAR imagery using a combination of feature-tracking and pattern-matching'

Stefan Muckenhuber and Stein Sandven

Nansen Environmental and Remote Sensing Center (NERSC), Thormøhlensgate 47, 5006 Bergen, Norway

Correspondence to: S. Muckenhuber (stefan.muckenhuber@nersc.no)

Dear Referee # 1,

Thank you very much for helping us improving our paper.

Please find here the **answers** to your comments and the corresponding ***changes in manuscript***:

1 Comments to the answers to Referee 1

Page 2 Line 42-46: The problem with the backscatter values is not solved by correcting a typo and claiming that the values were shown in Bell (a very uncommon unit for backscatter by the way). The correction of the typo shifts the backscatter values into the right magnitude. However, given a noise level of 22 dB for Sentinel-1 I would still like to question the calibration routines used. Using scaling suggested by the authors on correctly calibrated S1 data would mean to focus on a value range mainly containing noise (-32.5 dB - -22 dB) and only partly containing potentially meaningful backscatter values in the range -22 dB to -18.86 dB. The authors might want to check again there calibration routines.

The way we understood the Sentinel-1 data is that -22 dB represents the maximum NESZ (Noise Equivalent Sigma Zero) and the NESZ depends on the incidence angle. The maximum NESZ is found at the lowest incidence angle, but the NESZ values decrease with increasing incidence angle, which means that values below -22 dB might contain useful information. (Otherwise around half of the pixels in Figure 1 would be below the noise level.) The algorithm is mainly sensitive to changes of the upper brightness boundary and less sensitive to the lower brightness boundary (see Muckenhuber et al. 2016). Muckenhuber et al. 2016 tuned the algorithm to find suitable brightness boundaries and we converted the corresponding backscatter values to dB. The lower boundary in Muckenhuber et al. 2016 was set to 0. Since it is impossible to convert 0 to dB, we looked into the backscatter distributions of images

over sea ice (e.g. Figure 1) and chose a value that includes the majority of the measured dB values. This means that our lower dB threshold is set to an even higher value than used in Muckenhuber et al. 2016.

Page 8 Line 245: the use of logarithmic scaling is the standard for all SAR based sea ice research and professional monitoring by universities, ice services and research institutes. But it is good to see that this promising approach uses dB scaling now as well.

We agree and just wanted to mention why we did not apply the linear pre-processing as suggested by Muckenhuber et al. 2016 for the feature-tracking approach.

Page 8 Line 255: I did not want to vote against parameter tuning or the validation using displacement vectors derived from satellite image pairs. Both instruments are extremely useful. I just thought that a validation using the same dataset originally used for tuning is not the best approach for an independent validation. It is a pity that the authors decided to skip both parts completely but then it is for sure the most effective approach to deal with my remark.

We agree that comparison against manually derived drift vectors represent an important tool for parameter tuning, but we hope that the new approach delivers an even better parameter set, because a higher number of satellite image pairs is now considered.

Page 9 Line 278 - 301 I like this new paragraph you added into section 5, but as far as I can say it does not consider the specific problem, I outlined in my question and they suggest to handle with this paragraph (the same search window size means different degrees of freedom depending on the time span between the two considered image acquisitions) - It does however discuss the general aspect of time span regarding the 'hard' 0.5 m/s maximum speed threshold but I guess, that's o.k.

It is true that the same search window size for short and long time spans between acquisitions, results in different degrees of freedom. Considering short time spans allows for a higher velocity adjustment in the pattern-matching step. However, more feature-tracking vectors are usually found on image pairs with shorter time spans, which reduces the search window sizes, and acts to a certain extent against the higher degree of freedom. Adjusting the search window according to the time span would add additional complexity to both the algorithm and the parameter tuning and needs more research on how the search window should be adjusted depending on the time span. We aim for a simple algorithm both for computational efficiency and easy open-source distribution to users and therefore hope that the simple approach to remove drift vectors above the maximum speed is sufficient to satisfy the users need for now. Our current and future efforts include the investigation of ice drift behaviour on different time scales to combine drift information from image pairs with different time spans. This work will hopefully help us to improve our understanding on how to adjust the pattern-matching search

window in the most meaningful way.

2 The article itself

2.1 General comments

The article improved a lot since the last time and the authors handled the comments of the reviewers in a very efficient manner. It reads like a completely new manuscript. Personally I think that the authors tend to use superlatives like 'optimize' or 'most meaningful' a bit too often given the flexibility of their approach (various changes between both versions) but nevertheless it seems to be on a right track now and worth being published in 'The Cryosphere' after major revisions. Within the frame of the revision it would however be necessary to discuss the differences of this paper to the recently published paper by Anton Korosov and Pierre Rampal for the same institute on the same topic: A.Korosov and P. Rampal (2017): 'A Combination of Feature Tracking and Pattern Matching with Optimal Parametrization for Sea Ice Drift Retrieval from SAR Data', Remote Sens. 2017, 9(3), 258; doi:10.3390/rs9030258, which looks quite similar to me. Personally, I think that this parallel publishing from the same institute is at least a bit unfortunate (even though I'm aware, that the manuscript at hand was originally submitted earlier than the now published article by Korosov and Rampal).

We replaced 'optimised' with *adjusted* and removed 'most meaningful' throughout the manuscript.

Regarding the recent publication from Korosov and Rampal 2017: The open-source character of the review process in TC and the open-source distribution of the presented algorithm make it impossible to compete with journals that have a review process of approximately 31 days plus 7 days until acceptance to publication (median values for papers published in Remote Sensing in 2016 from http://www.mdpi.com/journal/remotesensing). Since the presented manuscript was earlier submitted and due to the fact that our manuscript and algorithm was already distributed in TCD and on github more than 2 months before the submission of Korosov and Rampal 2017, we would like to disregard the paper from Korosov and Rampal 2017 in our manuscript.

2.2 Specific comments

Page 4 Line 113-115 I'm not sure how much of the vector independence from the feature tracking actually exists, given the overlap of features from the various resolution levels, the filtering and polynomial least square fitting to identify outliers and the linear interpolation to get first guess estimates for the subsequent pattern matching. What do the authors think?

In this sentence, we refer to the feature-tracking vectors as such (blue in Figure 3), without considering filtering, fitting etc. The mentioned independence here is only reduced by overlapping, i.e. in the case of very close features. All other feature-tracking vectors can be seen completely independent from each other. We try to preserve this independence as good as possible during filtering and interpolation. The filter parameters were set according to our experience with the algorithm performance and visual interpretation of several representative image pairs. We tried to allow for the largest possible degree of freedom without including too many erroneous vectors. The first guess is constructed by triangulating the input data and performing linear barycentric interpolation on each triangle. Hence, the first guess is only affected by the three closest vectors and reveals therefore a relatively high degree of independence compared to methods that apply e.g. a pattern-matching resolution pyramid. The interpolation method was chosen in order to allow for as much independence as possible in the first guess. Our next goal is to test the algorithm on large datasets to identify potential weaknesses in areas with strong deformation, shear zones etc. and this work will provide further information on the independence of the final drift vectors.

Page 6 Line 173-192 I would like to repeat my statement from the last review: there seems to be something wrong with your calibration routine and it is not only a typo. It would be great for sea ice research if S1 had a sensitivity of -32.5 of even -25 dB only but its noise level is at -22 dB, which means that especially your lower boundaries for the scaling cause a problem for correctly calibrated S1 images.

See the first comment in Comments to the answers to Referre 1.

Page 6 Line 186 The scaling to 8 bit / 256 grey level is an input requirement for feature tracking using the ORB algorithm but reduces the signal variation. This reduces the effectiveness of the NCC which can handle any numerical precision you like. It is not a problem for medium to larger resolutions (like CMES service provided by the DTU) since there are still enough pixel in each correlation window but as soon as you go to higher resolutions, even slight variations in the signal become more important (since there might be not so many clear variations left in a smaller window). Have the authors tried to use the original dB backscatter values for the pattern matching instead of the scaled 256 greyscale image?

We thought about applying another scaling for the pattern-matching step, but decided to use the same scaling as used for feature-tracking for the following three reasons:

1. **Applying an additional conversion from the digital numbers (provided in the Sentinel-1 file) into dB values in a 32 bit floating point format increases the computational effort of the pre-processing step.**

2. **The utilised pattern-matching python package can handle both 8-bit and 32-bit floating-point format. However, using 32-bit increases the computational effort of the pattern-matching step.**

3. **The scaling that is currently applied was tuned to provide a high number of feature-tracking vectors. We assume that a scaling that favours the recognition of features is also favourable for the applied pattern-matching procedure.**

Page 9, Line 223-224 As I mentioned before, the use of logarithmic scaling for SAR is common and I'm actually surprised that the authors did not do it from the start.

We agree that logarithmic scaling represents the common procedure for SAR. We mention the procedure in this line to address the differences to the approach from Muckenhuber et al. 2016.

II Filters: I have various questions:

1. For the polynomial fit the authors use all vectors (those from coarser resolution levels and those from finer resolution levels - a single pixel on the coarser resolution level covers about 3.6 pixel on the finest resolution level: subpixel uncertainty of +/-145 m vs a subpixel uncertainty of +/- 40 m?) - isn't this a bit of a problem if you merge it all in one polynomial surface and then try calculate if the predicted vector is 100 px away from your polynomial surface?

Since we down-sample the image by a factor of two, the pixels have a size of 80 m and 287 m for the highest and lowest resolution level. The resolution levels are only considered inside the ORB python package and retrieving the information from which resolution level the vector is derived, is unfortunately not implemented at the moment. A work around would be to downsample the satellite image with Nansat and apply the feature-tracking algorithm individually for each resolution pyramid. However, that would increase the computational effort significantly and the vectors from the different resolution levels would not be linked and compared to each other in terms of Harris corner measure etc. This means that we have to treat all vectors equally regardless of the resolution level (since we don't know the resolution level). The threshold of 100 pixels in this context refers to 8 km away from the simulated starting point, since we work with a resolution of 80 m outside the feature-tracking procedure.

2. You are applying a least square fit to an angle and calculate a polynomial surface from it. How do you handle the zero-crossing problem and all the other problems you are facing once you start averaging and interpolating angle values?

We agree that the issue of zero-crossing during filter and inter-/extrapolation of the angle values needs to be addressed. We added a function that centres the feature-tracking rotations around 180° before filter and inter-/extrapolation and we remove the adjustment after filter

and inter-/extrapolation has been applied. The following has been added to Section 3.2 in II Filter:

To avoid zero-crossing issues during the following filter and inter-/extrapolation process (in case the image rotation δ between SAR_1 and SAR_2 is close to $0°$), a factor $|180-\delta|$ is added to the raw rotation values $\alpha_{raw\,f}$ using the following Equation:

$$\alpha_f = \begin{cases} \alpha_{raw\,f} + |180-\delta| & \textit{if } \alpha_{raw\,f} + |180-\delta| < 360 \\ \alpha_{raw\,f} + |180-\delta| - 360 & \textit{if } \alpha_{raw\,f} + |180-\delta| > 360 \end{cases} \quad (1)$$

This centres the reasonable rotation values in the proximity of $180°$. After applying the filter and inter-/extrapolation process, the estimated rotation α is corrected by subtracting $|180-\delta|$.

The following has been added to Section 3.2 in III First Guess:

As mentioned above, the rotation estimates α are now corrected for the adjustment applied in Equation 3, by subtracting $|180-\delta|$.

3. It seems that your angular polynomial surface has a peak at about 130°. Just for curiosity: Is this the rotation between both images?

In this case, the rotation between the two images is 129.08° and the mean feature rotation is 132.24°. The peak of the rotation distribution is usually close to the image rotation.

Page 11 Line 272-273: least square fit and linear function for angles? How do the authors handle the specific problems related with this (see my comments on II Filters)

We agree, that this issue needs to be addressed. See answer above to second comment under II Filters.

Page 11 Line 285-287: 'The uncertainty ... vector' I would claim that it is not the uncertainty of the estimate but the representativeness of the estimate and that it does not only depends on the distance to the next feature tracking based vector but as well on the heterogeneity of the other surrounding feature tracking based drift vectors.

We agree that the distance d indicates the representativeness rather than the uncertainty and changed the sentence to:

The representativeness of this estimate however, depends on the distance d to the closest feature-tracking vector.

We consider only the distance and not the heterogeneity of the surrounding feature-tracking vectors to be as computational efficient as possible. Our first attempt to estimate the drift at any given location on SAR_1, was to apply a search mechanism to identify the surrounding feature-tracking vectors. This procedure would allow to derive a search window size based on the heterogeneity of the surrounding vectors. However, this approach was computationally

very inefficient. Our current method to derive a matrix that includes the distances to the closest location of a feature-tracking vector and the applied extra-/interpolation procedure are implemented in a computational efficient manner in the python toolbox SciPy. This allows us to derive drift estimates for the entire scene in a few minutes. The computational efficiency of the algorithm is one of our main goals, since we want to derive sea ice drift from large datasets and prepare for an operational product.

Page 12 Line 307-308: As far as I know the idea to restrict the smaller correlation template to a circle has been strongly propagated by Roberto Saldo from the DTU who uses it for his drift algorithm. I'm not sure if this is what the authors mean. While I'm aware of the advantages to limit the smaller correlation template to a circle, I have no idea why you would want to restrict your search window to a circle (if not only for the reason to safe computation) but may be the authors want to outline the advantages of a circled search window while having a rectangular correlation template. If they meant to describe a circled correlation window the authors want to refer to Roberto Saldo (if there is no publication regarding this matter may be as personal communication).

Here we refer to the larger search window t_2 on SAR_2 and not to the small template t_1 on SAR_1 around the start position of the vector.

From the public discussion, we understood that Referee #2 wanted circular templates for both the small and large template. See comment:

'P7 Fig.2 (and text): Why rectangular/square templates has been used? A circular template would be much easier (symmetric) to rotate. Consider using a circular templates instead.'

And our answer from 13.02.2017:

'We agree with this comment. Regarding t_1 however, the current version of the used OpenCV function matchTemplate does not allow circular templates and work-arounds would influence the result and the computational efficiency. We hope that a later version of matchTemplate will allow to use masks. Regarding t_2, we included a circular mask for the matching result to limit the search area to a circle rather than a square.'

To us, it seems more reasonable to search in a circular area rather than a square. This limits the distance from the first guess to a constant value, rather than to an arbitrary value depending on the looking angle of the satellite. This should also be beneficial when searching for a suitable size for the search window. If there is a correct match in the corner of a square during parameter tuning, a size for t_2 might be recommended that is too small considering another looking angle of the satellite.

We added the following sentence:

This limits the distance from the first guess to a constant value, rather than to an arbitrary value depending on the looking angle of the satellite.

Page 13 Line 318-319: 'In order to be consistent with the resolution of the feature tracking'. What is the advantage of being consistent with the resolution of the feature tracking?

Sea ice drift might be different on different resolution scales. This is particularly an issue in the case of rotation. The feature-tracking vectors provide the first guess and this vector field should represent the same drift resolution as considered by the pattern-matching step.

Also, during the tuning of the feature-tracking algorithm, we found the considered template size to be a good compromise between high resolution and capturing enough information for a reliable recognition performance. We assume that this also means that the template size represents a good choice for the pattern-matching step.

Page 14 Line 344-352 A higher MCC value seems to indicate a higher chance of a better match for your algorithm compared to buoy data. This is an interesting finding since most pattern matching algorithms have lower MCC_min values or none at all and since it was shown, that there is no direct relation between error and correlation coefficient.

This could mean that the author's initial guess and search strategy are less effective than those of pure pattern matching algorithms (and thereby needing a higher correlation to find a suitable match) especially since the maximum shift from the feature tracking based first guess is 1.6 (d=10) to 16 km (d=100) at maximum. Every difference above that is a hint that the first guess did not work or that the buoy drift has nothing to do with the surrounding ice conditions (Figure 11 a). Additionally I suggest checking the spatial distribution of the vectors the authors rejected due to their low MCC and high spatial distance (e.g. a shearing zone within the correlation window would for example cause as well a drop in the correlation value and potentially a larger difference in displacement relatively to an originally close drift buoy in another drift regime) and study the behavior compared to manually tracked vectors from the image pair ensure that the difference comes really from the algorithm and not from the limitations of the comparison with buoys, the authors are well aware of (page 20 line 439 - 450).

It is correct, that the drift vectors with higher cross correlation provided by our algorithm match better with the buoy drift than the vectors with low MCC values.

We believe that our initial guess provides a reliable estimate for the following reasons:

Initial guess in the proximity of the feature-tracking vectors: The error of the feature-tracking vectors is in the order of a few 100 m compared to manually derived vectors, as shown by Muckenhuber et al. 2016. This error does not prohibit the pattern-matching step to search at the correct location.

Initial guess further away from feature-tracking vectors: Every distance D above 16 km indicates that the first guess was not close enough to the buoy position, to allow the pattern-matching to search for a match at the buoy location. However, only very few points are above this limit and the buoy location does not necessarily represent the same ice drift as

the algorithm. As shown in Section 4.1 'Search restrictions evaluation', increasing the search window and allowing up to 200 pixels deviation from the first guess, did not provide many additional vectors with a distance D below 1000 m. Therefore we believe that the search window restrictions are suitable for our area and time period of interest.

Increasing the search window can also increase the error potential, in case the initial guess is correct. E.g. in very homogeneous ice conditions the pattern-matching could fail and accept a random match. In this case, the search window restricts the deviation from the first guess and hereby the error potential.

There is certainly a small remaining probability that the first guess is far away from the correct location and the search window is too small to include the correct location. We tried to find a good compromise between minimising this probability and being computational efficient enough to perform high resolution drift analysis within a few minutes.

We believe that the presented approach outperforms pure pattern-matching procedures in terms of computational effort while, at the same time, allowing for higher drift and rotation deviation in the drift field. A simple pattern-matching approach with no restrictions is certainly not computational efficient to provide high-resolution ice drift from a large satellite database. Therefore, pure pattern-matching approaches usually apply a resolution pyramid to limit the computational power, which means that high resolution estimates are based on low resolution drift. This, in combination with additional filtering and smoothing that is usually applied to discard outliers, decreases the independence of the high-resolution drift vectors significantly.

The initial guess of our approach builds on feature-tracking vectors that may point in any direction regardless of the neighbouring vector and may include any rotation from 0 to 360°. During the filter and inter-/extrapolation process, we try to preserve the high degree of independence to allow for relatively strong deviation in terms of drift and rotation.

We did not reject matches according to high spatial distance, but only based on the MCC value.

We changed Figure 8 to illustrate the spatial distribution of accepted and rejected vectors and added the following sentence to the caption:

Green and blue colour indicates start locations (on SAR_1) to which the algorithm provided vectors with a MCC value above and below 0.4 using (a) HV and (b) HH polarisation.

As shown in the first draft of the manuscript, we compared the algorithm results with manually derived drift vectors and found that the results compared well. According to the previous comments, we removed the comparison with the manually derived drift vectors and decided to use the buoy data also for parameter evaluation to increase the size of the dataset and cover a larger range of ice conditions, time spans etc.

As stated in the discussion, the recommended parameters are not meant as a fixed setting,

but should rather give a suggestion and guideline to estimate the expected results and the corresponding computational effort. They can easily be varied in the algorithm setup and should be chosen according to the needs of the user. To provide an improved parameter setting depending on ice conditions, area of interest etc. and further test and adjust the initial guess procedure, the next step of our research is to apply the algorithm on large datasets.

Page 15 3.3 Comparison with buoy data: Just for my understanding: Did the authors center a 34x34 pixel window at the original buoy position? The original buoy position has been acquired every hour or has been interpolate to hourly intervals

Yes, a 34×34 pixel window was centred around the buoy start position. Based the conversation with Polona Itkin and Gunnar Spreen, most buoys acquired the GPS position every hour, but some every three hours. In the later case, the positions were interpolated to every hour by NPI.

Page 15 Line 356 'Each pair yielded more than ... three days' I'm not sure but it would probably more interesting to mention the number of vectors, which the recent version of the feature tracking component provides, using HV only and dB scaling, if at all ...

We used the recent version of our feature-tracking algorithm and changed the sentence to: ***Each pair yielded more than 300 drift vectors applying the feature-tracking algorithm from Section 3.2 and had a time difference between the two acquisitions of less than three days.***

Page 17 Figure 9 and 10: Based on the Figures it is difficult to see an advantage for the variation of the search window size or the rotation angle aside from computational efficiency. Would the authors agree?

The computational efficiency is an important argument for the variation of the restrictions (search window and rotation angle). In addition, several red dots which where closer than 100 pixels ($d < 100$ pixels) are excluded by applying the recommended restrictions. Apparently, a large pattern-matching adjustment close to a feature-tracking vector increases the possibility of an error (represented by $D > 1000$ m). We assume that in these cases, the initial guess provided already a good estimate and a large search window and rotation range rather increases the error potential.

Page 18 Fig 11 a: something seems to be wrong with the legend

We adjusted the legends in Figure 11 according to this comment.

Page 18 Fig 11 b: how would the fit look like if the authors would include the values you rejected due to their low correlation value?

We included a logarithmic normal distribution for all results and changed the sentence in the caption to the following:

Logarithmic histogram of distance D ***with 100 bins between 10 m and*** 10^5 ***m including two logarithmic normal distributions that were fitted to all results (grey) and to the filtered results with*** $MCC > 0.4$ ***(solid red line).***

Page 18 Line 407 / Page 20 Line 441 'median and 341.9 m' What's the significance? Obviously it means that 50% of your data has an error of less than 340 m with respect to the buoy data but it means as well that 50% have an error, that is larger (and based on the distribution: 1% < 20m, 5% < 43m, 10% < 68m, 68% (1 sigma criterion) < 620 m, 95% (2 sigma criterion) < 2700 m and 99% (3 sigma criterion) < 6400m). But could the authors give a hint what it could mean regarding the quality of the algorithm, given the various influences they identified which could have biased the result? May be a solution would again be to use the manually derived vectors from the original draft for it to account for the algorithm 'accuracy' only (well with an 'uncertainty' hidden in the manually collected drift vectors of course)?

According to the comment of Referee #2 during the first review process, 'the validation with this data set (NB: the manually derived vectors) is not fair as the algorithm has been tuned for this data. Then only the buoy data can be used for independent validation.' Therefore, we had to excluded the comparison with the manually derived vectors. In addition, the buoy dataset represents a larger dataset, accounts for a larger range of ice conditions and time spans and is therefore more representative for our area and time period of interest, despite its limitations.

Page 20 Line 458-460 'The parameters can ... strong rotation).' I have a fair idea which parameters to vary to meet changes in computational power, area of interest and expected ice conditions but I have no idea why availability of time, computational power and number of image pairs are mentioned individually since the only parameter behind it is computation time or rather the selection of a finer or coarser resolution. Additionally I would be interested what parameter to change to influence the accuracy!

We meant resolution instead of accuracy and changed the sentence to the following:

The parameters can easily be varied in the algorithm setup and should be chosen according to availability of computational power, needed resolution, area of interest and expected ice conditions (e.g. strong rotation).

Page 20 Line 470-484 I guess this paragraph is based on information you received from Nuno Miranda. It would be useful to refer to it as Personal Communication in the text since otherwise the readers might wonder where this information comes from.

Yes, this paragraph is based on a personal communication with Nuno Miranda and we added the following to the end of the paragraph:

(Personal Communication with Nuno Miranda, January 2017)

Page 21 Line 487-490 'Our next step ... less than 5 km' That's really nice! I'm really looking forward to such a dataset with a good quality. However, given that most of the S1-data in the Arctic and Antarctic is in HH polarization (in Antarctica completely) wouldn't it been better to perform this study in HH from the beginning, even if there seems to be an advantage for HV in the feature tracking?

So far, we found good coverage in HV for our area and time period of interest. However, it is true that some areas are currently only monitored in HH and we included an algorithm performance evaluation also for HH polarisation.

We changed the sentence to:

Our next step is to embed the algorithm into a super-computing facility to further test the performance in different regions, time periods and ice conditions and evaluate and combine the results of different polarisation modes.

We aim to eventually combine drift information from the two channels in the most meaningful way. This is also described further down in Section 5 'Discussion and outlook'. We expect that the number of feature-tracking vectors derived from HH will increase in the future due to an increased coverage provided by Sentinel-1A and Sentinel-1B (a shorter time span between the acquisitions is favourable for HH as shown by Muckenhuber et al. 2016) and a better pre-processing system that we will be able to access through our ongoing cooperation with TU Wien. This will bring the feature-tracking performance of HH closer to the performance of HV and therefore the same (or a very similar) parameter setting is expected to be favourable for HH.

Page 21 Line 503 'better coverage in HH pol' - that's nicely put - the S1 observation scenario does not plan any HV acquisition Antarctic part of the southern ocean and none in the central Arctic ocean but it could of be a reason to demonstrate the need for HV data in these regions as well.

We changed the sentence to:

We found our area of interest well covered with HV images, but other areas in the Arctic and Antarctic are currently only monitored in HH polarisation.

We agree, that the shown HV performance to track features could demonstrate the need for HV data in regions that are currently only monitored in HH. However, before we suggest to monitor these regions with HV, we would like to compare the two channels more thoroughly and perform case studies in the respective regions. Based on the presented work we can only refer to our area and time period of interest, which is well covered with HV data. Testing the

algorithm on large HV and HH datasets will hopefully provide us with more information on the necessity of HV monitoring for sea ice drift retrieval.

Page 21 Line 507 - 510 'Therefore ...future work' A good idea! Just a thought I would like to add. Feature tracking needs linear features which tend to depend a bit more on incidence angle, orbit, and changes in ice condition in HH than in HV and depending on the robustness of your feature detector it might even be quite robust to the quite strong noise in the S1-HV data (it is actually impressive how many feature tracking based vectors you were able to retrieve from the HV scene compared to the HH one). This could explain the better performance of the feature tracking part for the HV component. Cross correlation based pattern matching however is less sensitive to changes in linear feature and more sensitive to areal pattern changes which might potentially favor the HH channel - but as I said: just a thought.

We agree and added the following to Section 5:

Another argument is that the presented feature-tracking approach identifies and matches corners, which represent linear features. The linear features on HH images are more sensitive to changes in incidence angle, orbit and ice conditions than the linear features on HV images. This could explain the better feature-tracking performance of the HV channel. However, pattern-matching is less affected by changing linear features and more sensitive to areal pattern changes. This could potentially mean that the HH channel performs better than HV when it comes to pattern-matching.

2.3 Technical comments

Page 1 Line 9 'pre-processing of S1 data ... has been optimized' - Are the authors refereeing to their use of the logarithmic scale for the backscatter again? As far as I'm aware that is all you did and it is a bit of disappointing if the abstract promises an optimized preprocessing while the article offers the conversion to dB only.

The sentence has been changed to:

The pre-processing of the Sentinel-1 data has been adjusted to retrieve a feature distribution that depends less on SAR backscatter peak values.

Page 1 Line 10-13 I'm not sure if computational efficiency is necessary in the abstract, the authors might want to give it a second thought but I'm fine if you want to keep it there.

In case the 'computational efficiency' in Line 6-7 is addressed by this comment, we would like to keep the phrase. Our long-term goals are an operational sea ice drift product and to provide large drift datasets. Therefore the computational efficiency of the algorithm is a ma-

jor factor for us and one of the main arguments for the development of the presented approach.

Introduction: I think the introduction improved a lot but especially of page 3 I miss something running like a common thread through it. It reads like an accumulation of independent facts.

We changed the introduction according to this comment. The history and evolution of sea ice drift retrieval from SAR is to a certain extent an accumulation of independent facts, since it includes the work of different people and institutes, but we tried to re-write the part in order to emphasize the connections.

Page 3 Line 69 If I'm not mistaken, Hollands and Dierking (2011) implemented their own modified version of the algorithm and did not just continue the work on the algorithm but the authors might want to check that.

We changed the sentence to:

Hollands and Dierking (2011) implemented their own modified version of this algorithm to derive sea ice drift from ENVISAT ASAR data.

Page 3 Line 86 -88 'Muckenhuber ... Sentinel-1 data' I suggest adding at the end of the sentence something like: 'as a frontend to the ORB algorithm from Rublee included in the OpenCV package' just to give the reader an impression of the used technique, but I might be mistaken.

We changed the sentence to:

This paper follows up the work from Muckenhuber et al. (2016), who published an open-source feature-tracking algorithm to derive computationally efficient sea ice drift from Sentinel-1 data based on the open-source ORB algorithm from Rublee et al. (2011), that is included in the OpenCV Python package.

Page 5 Line 139 'HV polarization' - given that most of the Arctic and the whole Antarctic is only covered by HH data this limits the conclusions for the application of the presented algorithm to the European Part of the Arctic and the Baltic sea.

We changed the sentence to:

However, the focus of this paper is put on using HV polarisation (mainly acquired over the European Arctic and the Baltic sea), since this channel provides in our area of interest on average four times more feature tracking vectors than HH (Muckenhuber et al., 2016), representing a better initial drift estimate for the combined algorithm.

Page 5 Line 165 'Nansat ... gdal.org).' It reads like a commercial - may be the authors want to give this line a second thought.

We changed the sentence to:

To process Sentinel-1 images within Python (extraction of backscatter values and corresponding geolocations, reprojection, resolution reduction etc.), we use the Python toolbox Nansat (Korosov et al., 2016), that builds on the Geospatial Data Abstraction Library (http://www.gdal.org).

Page 9, Line 215 I suggest to add :'Given a suitable threshold [and unique features]...'

We agree and changed the sentence accordingly.

Page 9, Line 217 I suggest to change: 'Muckenhuber ... found the most suitable ...' to 'Muckenhuber ... found a suitable ...' given the flexibility of your approach and your suggested parameters

We agree and changed the sentence accordingly.

Page 10 Line 260-261: I suggest adding something like: 'The quality of this 'first guess', however depends on the density of the feature vector field and the local ice conditions'

We added the following sentence after the first sentence in Section 'III First guess':

The quality of this 'first guess', however depends on the density of the feature-tracking vector field and the local ice conditions.

Please find attached the corrected manuscript with changes marked in blue and red.

Thanks again for your comments. We are looking forward to your reply!

Best regards,

S. Muckenhuber and S. Sandven

Manuscript prepared for J. Name
with version 2015/09/17 7.94 Copernicus papers of the LaTeX class copernicus.cls.
Date: 2 May 2017

Response to Referee # 2

'Open-source sea ice drift algorithm for Sentinel-1 SAR imagery using a combination of feature-tracking and pattern-matching'

Stefan Muckenhuber and Stein Sandven

Nansen Environmental and Remote Sensing Center (NERSC), Thormøhlensgate 47,
5006 Bergen, Norway

Correspondence to: S. Muckenhuber (stefan.muckenhuber@nersc.no)

Dear Referee # 2,

Thank you very much for helping us improving our paper.

Please find here the **answers** to your comments and the corresponding ***changes in manuscript***:

Comments

P13 (in the version with the changes indicated): 'normalized cross coefficient', I think this should be 'normalized cross-correlation coefficient' or just 'normalized cross-correlation', Check this throughout the manuscript, I think this appears more than once.

We changed 'cross coefficient' to *cross-correlation* throughout the manuscript.

Eq 11: One closing parenthesis missing "argmax(NCC(x,y)" -> agrmax(NCC(x,y)). Could also add (x,y) under argmax to indicate that argmax is with respect to (x,y).

We changed Equation 11 to the following:

$$(\frac{1+t_{s2}-t_{s1}}{2}+dx, \frac{1+t_{s2}-t_{s1}}{2}+dy) = \underset{x,y}{argmax}(\mathbf{NCC}(x,y)) \quad (1)$$

Please find attached the corrected manuscript with changes marked in blue and red.

Thanks again for your comments. We are looking forward to your reply!

Best regards,

S. Muckenhuber and S. Sandven

Manuscript prepared for J. Name
with version 2015/09/17 7.94 Copernicus papers of the LaTeX class copernicus.cls.
Date: 2 May 2017

Open-source sea ice drift algorithm for Sentinel-1 SAR imagery using a combination of feature-tracking and pattern-matching

Stefan Muckenhuber and Stein Sandven

Nansen Environmental and Remote Sensing Center (NERSC), Thormøhlensgate 47,
5006 Bergen, Norway

Correspondence to: S. Muckenhuber (stefan.muckenhuber@nersc.no)

Abstract. An open-source sea ice drift algorithm for Sentinel-1 SAR imagery is introduced based on the combination of feature-tracking and pattern-matching. Feature-tracking produces an initial drift estimate and limits the search area for the consecutive pattern-matching, that provides small to medium scale drift adjustments and normalised ~~cross coefficient~~ cross-correlation values. The algorithm is designed to combine the two approaches in ~~the most meaningful way in~~ order to benefit from the respective advantages. The main advantages of the considered feature-tracking approach are the computational efficiency and the independence of the vectors in terms of position, lengths, direction and rotation. Pattern-matching on the other side allows better control over vector positioning and resolution. The pre-processing of the Sentinel-1 data has been ~~optimised~~ adjusted to retrieve a feature distribution that depends less on SAR backscatter peak values. Applying the algorithm with the recommended parameter setting, sea ice drift retrieval with a vector spacing of 4 km on Sentinel-1 images covering 400 km x 400 km, takes about 4 minutes on a standard 2.7 GHz processor with 8 GB memory. The corresponding recommended patch size for the pattern-matching step, that defines the final resolution of each drift vector is 34×34 pixels (2.7×2.7 km). For validation, calculated drift results from ~~241~~ 246 Sentinel-1 image pairs have been compared to buoy GPS data, collected in 2015 between 15^{th} January and 22^{nd} April and covering an area from 80.5° N to 83.5° N and 12° E to 27° E. We found a logarithmic normal distribution of the error with a median at ~~341.9~~352.9 m using HV polarisation and 535.7 m using HH polarisation. All software requirements necessary for applying the presented sea ice drift algorithm are open-source to ensure free implementation and easy distribution.

1 Introduction

Sea ice drift has a strong impact on sea ice distribution on different temporal and spatial scales. Motion of sea ice due to wind and ocean currents causes convergence and divergence zones, resulting in formation of ridges and opening/closing of leads. On large scales, ice export from the Arctic and

Antarctic into lower latitudes, where the ice eventually melts away, contributes to a strong seasonality of total sea ice coverage (IPCC, 2013). Due to a lack of ground stations in sea ice covered areas, satellite remote sensing represents the most important tool for observing sea ice conditions on medium to large scales. Despite the strong impact of sea ice drift and the opportunities given by latest satellite remote sensing techniques, there is a lack of extensive ice drift data sets providing sufficient resolution for estimating sea ice deformation on a spatial scaling of less than 5 km.

Our main regions of interest are the ice covered seas around Svalbard and East of Greenland. Characteristic for this area are a large variation of different ice types (Marginal Ice Zone, First Year Ice, Multi Year Ice etc.), a strong seasonality of ice cover and a wide range of drift velocities. Focus was put on the winter/spring period, since the area of interest experiences the highest ice cover during this time of the year.

Early work from Nansen (1902) established the rule-of-thumb that sea ice velocity resembles 2 % of the surface wind speed with a drift direction of about 45° to the right (Northern Hemisphere) of the wind. This wind driven explanation can give a rough estimate for instantaneous ice velocities. However, the respective influence of wind and ocean current strongly depends on the temporal and spatial scale. Only about 50 % of the long-term (several months) averaged ice drift in the Arctic can be explained by geostrophic winds, whereas the rest is related to mean ocean circulation. This proportion increases to more than 70 % explained by wind, when considering shorter time scales (days to weeks). The wind fails to explain large-scale ice divergence patterns and its influence decreases towards the coast (Thorndike and Colony, 1982).

Using GPS drift data from the International Arctic Buoy Program (IABP), Rampal et al. (2009) analysed the general circulation of the Arctic sea ice velocity field and found that the fluctuations follow the same diffusive regime as turbulent flows in other geophysical fluids. The monthly mean drift using 12 h displacements was found to be in the order of 0.05 to 0.1 m/s and showed a strong seasonal cycle with minimum in April and maximum in October. The IABP dataset also revealed a positive trend in the mean Arctic sea ice speed of +17 % per decade for winter and +8.5 % for summer considering the time period 1979–2007. This is unlikely to be the consequence of increased external forcing. Instead, the thinning of the ice cover is suggested to decrease the mechanical strength which eventually causes higher speed given a constant external forcing (Rampal et al. , 2009b).

Fram Strait represents the main gate for Arctic ice export and high drift velocities are generally found in this area with direction southward. Based on moored Doppler Current Meters mounted near 79° N 5° W, Widell et al. (2003) found an average southward velocity of 0.16 m/s for the period 1996–2000. Daily averaged values were usually in the range 0–0.5 m/s with very few occasions above 0.5 m/s.

GPS buoys and Current Meters are important tools to measure ice drift at specific locations. However, to monitor sea ice drift on medium to large scales, satellite remote sensing represents the most important data source today. The polar night and a high probability for cloud cover over

sea ice limit the capability of optical sensors for reliable year-round sea ice monitoring. Space-borne Synthetic Aperture Radar (SAR)~~are~~ , on the other hand, are active microwave sensors and can produce high resolution images regardless of solar illumination and cloud cover. Since the early 1990's SAR sensors are delivering systematic acquisitions of sea ice covered oceans ~~since the early 1990's~~ and Kwok et al. (1990) showed that sea ice displacement can be calculated from consecutive SAR scenes. ~~SAR is an active imaging sensor operating in the microwave spectrum and produces data regardless of solar illumination and cloud cover.~~

The geophysical processor system from Kwok et al. (1990) has been used to calculate sea ice drift fields in particular over the Western Arctic (depending on SAR coverage) once per week with a spatial resolution of 10-25 km for the time period 1996–2012. This extensive dataset makes use of SAR data from RADARSAT-1 operated by the Canadian Space Agency, and from ENVISAT (Environmental Satellite) ASAR (Advanced Synthetic Aperture Radar) operated by ESA (European Space Agency). ~~A~~

To resolve drift details on a finer scale, a high-resolution sea ice drift algorithm for SAR images from ERS-1 (European Remote-sensing Satellite from ESA) based on pattern-matching was introduced by Thomas et al. (2008), ~~allowing drift calculation~~ that allowed drift calculation with up to 400 m resolution. ~~The work on this algorithm has been continued by Hollands and Dierking (2011) , who derived~~ Hollands and Dierking (2011) implemented their own modified version of this algorithm to derive sea ice drift from ENVISAT ASAR data.

To provide drift estimates also in areas where areal matching procedures (like cross and phase correlation) fail, Berg and Eriksson (2014) introduced a hybrid algorithm for sea ice drift retrieval from ENVISAT ASAR data using phase correlation and a feature based matching procedure that is activated if the phase correlation value is below a certain threshold.

The current generation of SAR satellites including RADARSAT-2 and Sentinel-1 are able to provide images with more than one polarisation. Komarov and Barber (2014) and Muckenhuber et al. (2016) have evaluated the sea ice drift retrieval performance ~~of dual-polarisation SAR imagery~~ with respect to the polarisation using a combination of phase/cross-correlation and feature-tracking based on corner detection respectively. Muckenhuber et al. (2016) has shown that feature-tracking provides on average around four times as many vectors using HV polarisation compared to HH polarisation. ~~Making use of Sentinel-1 SAR data, an operational sea ice drift product with 10km resolution is provided by the Danish Technical University (Pedersen et al. (2015) , http://www.seaice.dk/) as part of the Copernicus Marine Environment Monitoring Service (CMEMS, http://marine.copernicus.eu).~~

After the successful start of the Sentinel-1 mission in early 2014, high-resolution SAR images are delivered for the first time in history within a few hours after acquisition as open-source data to all users. This introduced a new era in SAR Earth observation with great benefits for both scientists and other stack holders. ~~The sea ice~~ Easy, free and fast access to satellite imagery

facilitate the possibility to provide products on an operational basis. The Danish Technical University (Pedersen et al. (2015) , http://www.seaice.dk/) provides an operational sea ice drift product based on Sentinel-1 data with 10 km resolution as part of the Copernicus Marine Environment Monitoring Service (CMEMS, http://marine.copernicus.eu).

The sea ice covered oceans in the European Arctic Sector represent an important area of interest ~~and with~~ for the Sentinel-1 mission and with having a revisit time of less than one day in the Arctic (ESA, 2012), our area of interest is monitored by Sentinel-1 on a daily basis. ~~Muckenhuber et al. (2016)~~

This paper follows up the work from Muckenhuber et al. (2016) , who published an open-source feature-tracking algorithm to derive computationally efficient sea ice drift from Sentinel-1 data ~~.~~ ~~This paper follows up the work from Muckenhuber et al. (2016) and aims~~ based on the open-source ORB algorithm from Rublee et al. (2011) , that is included in the OpenCV Python package. We aim to improve the feature-tracking approach by combining it with pattern-matching. Unlike Berg and Eriksson (2014), the feature-tracking step is performed initially and serves as a first guess to limit the computational effort of the pattern-matching step.

~~Contemporary~~ From a methodological point of view, algorithms for deriving displacement vectors between two consecutive SAR images are based either on feature-tracking or pattern-matching.

Feature-tracking detects distinct patterns (features) in both images and tries to connect similar features in a second step without the need for knowing the locations. This can be done computationally efficient and the resulting vectors are often independent of their neighbours in terms of position, lengths, direction and rotation, which is an important advantage for resolving shear zones, rotation and divergence/convergence zones. The considered feature-tracking approach identifies features without taking the position of other features into account and matches features from one image to the other without taking the drift and rotation information from surrounding vectors into account (Muckenhuber et al., 2016). However, due to the independent positioning of the features, very close features may share some pixels and since all vectors from the resolution pyramid are combined, the feature size varies among the matches, which implies a varying resolution. In addition, the resulting vector field is not evenly distributed in space and large gaps may occur between densely covered areas, which can eventually lead to missing a shear or divergence/convergence zone.

Pattern-matching, on the other hand, takes a small template from the first image at the starting location of the vector and tries to find a match on a larger template from the second image. Despite a considerable computational effort, this approach is widely used, since it allows to define the vector positions. For practical reasons, a pyramid approach is generally used to derive high-resolution ice drift. This speeds up the processing, but limits the independence of neighbouring vectors, since they depend on a lower resolution estimate (Thomas et al., 2008).

The objective of this paper is to combine the two approaches in ~~the most meaningful way in~~ order to benefit from the respective advantages. The main advantages of the considered feature-

tracking approach are the computational efficiency and the independence of the vectors in terms of position, lengths, direction and rotation. Pattern-matching on the other side allows better control over vector positioning and resolution, which is a necessity for computing divergence, shear and total deformation.

The presented algorithm, all necessary software requirements (python incl. Nansat, openCV and SciPy) and the satellite data from Sentinel-1 are open-source. A free and user friendly implementation shall support an easy distribution of the algorithm among scientists and other stakeholders.

The paper is organised as follows: The used satellite products and buoy data are introduced in Section 2. The algorithm description including data pre-processing is given in Section 3, together with tuning and validation methods. Section 4 presents the pre-processing, parameter tuning and validation results and provides a recommended parameter setting. The discussion including outlook can be found in Section 5.

2 Data

The Sentinel-1 mission is a joint initiative of the European Commission and the European Space Agency (ESA) and represents the Radar Observatory for the Copernicus Programme, a European system for monitoring the Earth with respect to environmental and security issues. The mission includes two identical satellites, Sentinel-1A (launched in April 2014) and Sentinel-1B (launched in April 2016), each carrying a single C-band SAR with a centre frequency of 5.405 GHz and dual-polarisation support (HH+HV, VV+VH) also for wide swath mode. Both satellites fly in the same near-polar, sun-synchronous orbit and the revisit time is less than 1 day in the Arctic (ESA, 2012). The main acquisition mode of Sentinel-1 over sea ice covered areas is Extra Wide Swath Mode Ground Range Detected with Medium Resolution (EW GRDM) and the presented algorithm is built for processing this data type. The covered area per image is 400 km × 400 km and the data are provided with a pixel spacing of 40 m × 40 m in both ~~HH and HV~~ HV and HH polarisation. The introduced algorithm can utilise both ~~HH and HV~~ HV and HH channel. However, the focus of this paper is put on using HV polarisation (mainly acquired over the European Arctic and the Baltic sea), since this channel provides in our area of interest on average four times more feature tracking vectors than HH (Muckenhuber et al., 2016), representing a better initial drift estimate for the combined algorithm.

To illustrate the algorithm performance and explain the individual steps, we use an image pair acquired over Fram Strait. The acquisition times of the two consecutive images are 2015-03-28 07:44:33 (UTC) and 2015-03-29 16:34:52 (UTC), and the covered area is shown in Figure 3. This image pair covers a wide range of different ice conditions (multiyear ice, first-year ice, marginal ice

zone etc.) and the ice situation is representative for our area and time period of interest.

To evaluate suitable search limitations and validate the algorithm, we use GPS data from drift buoys that have been set out in the ice covered waters north of Svalbard as part of the Norwegian Young Sea Ice Cruise (N-ICE2015) project of the Norwegian Polar Institute (Spreen and Itkin, 2015). The ice conditions during the N-ICE2015 expedition are describe on the project website (http://www.npolar.no/en/projects/n-ice2015.html) as challenging. The observed ice pack, mainly consisting of 1.3-1.5 m thick multiyear and first-year ice, drifted faster than expected and was very dynamic. Closer to the ice edge, break up of ice floes has been observed due to rapid ice drift and the research camp had to be evacuated and re-established four times. This represents a good study field, since these challenging conditions are expected in our area and time period of interest. The considered GPS data have been collected in 2015 between 15^{th} January and 22^{nd} April, and cover an area ranging from 80.5° N to 83.5° N and 12° E to 27° E. The buoys recorded their positions either hourly or every three hours. In the later case, the positions have been interpolated for each hour.

3 Method

3.1 Data pre-processing

To process Sentinel-1 images within Python (extraction of backscatter values and corresponding geolocations, reprojection, resolution reduction etc.), we use the ~~open-source software Nansat (Korosov et al., 2016) . Nansat is a scientist-friendly Python toolbox for 2-D satellite Earth observation data, and~~ Python toolbox Nansat (Korosov et al., 2016) , that builds on the Geospatial Data Abstraction Library (http://www.gdal.org). As done in Muckenhuber et al. (2016), we change the projection of the the provided ground control points (latitude/longitude values given for certain pixel/line coordinates) to stereographic and use spline interpolation to calculate geographic coordinates. This provides a good geolocation accuracy also at high latitudes. The pixel spacing of the image is changed by averaging from 40 m to 80 m, which is closer to the sensor resolution of 93 m range × 87 m azimuth, and decreases the computational effort.

For each pixel p, the Sentinel-1 data file provides a digital number DN_p and a normalisation coefficient A_p, from which the normalised radar cross section σ^0_{raw} is derived by the following equation:

$$\sigma^0_{\text{raw}} = DN_p^2/A_p^2 \tag{1}$$

The normalised radar cross section σ^0_{raw} reveals a logarithmic distribution and the structures in the sea ice are mainly represented in the low and medium backscatter values rather than in the highlights. Therefore, we change the linear scaling of the raw backscatter values σ^0_{raw} to a logarithmic scaling and get the backscatter values $\sigma^0 = 10 * \lg(\sigma^0_{\text{raw}})$ [dB]. A representative backscatter distribution over

sea ice is shown in Figure 1. Using a logarithmic scaling provides a keypoint distribution for the feature tracking algorithm that depends less on high peak values, while the total number of vectors increases.

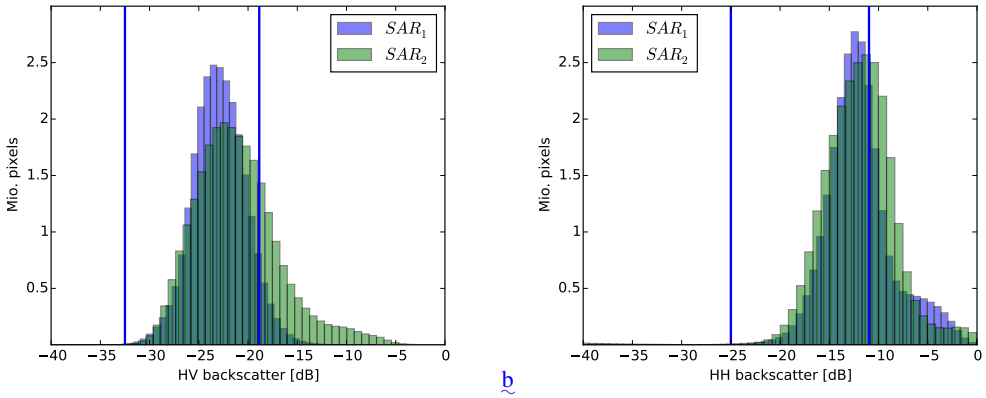

Figure 1. Histogram of (a) HV and (b) HH backscatter values σ^0 from image pair Fram Strait. The lower and upper brightness boundaries for HV ($\sigma^0_{\text{min}} = -32.5$ dB~~and~~, $\sigma^0_{\text{max}} = -18.86$ dB) and HH ($\sigma^0_{\text{min}} = -25.0$ dB, $\sigma^0_{\text{max}} = -10.97$ dB) are shown with blue lines and illustrate the domain for the intensity values i.

To apply the feature-tracking algorithm from Muckenhuber et al. (2016), the SAR backscatter values σ^0 have to be converted into intensity values i with $0 \leq i \leq 255$ for $i \in \mathbb{R}$. This conversion is done by using Eq. (2) and setting all values outside the domain to 0 and 255.

$$i = 255 \cdot \frac{\sigma^0 - \sigma^0_{\text{min}}}{\sigma^0_{\text{max}} - \sigma^0_{\text{min}}} \tag{2}$$

The upper brightness boundary σ^0_{max} is set according to the recommended value from Muckenhuber et al. (2016), i.e. -18.86 dB and -10.97 dB for HV and HH respectively. The lower boundary σ^0_{min} was chosen to be -32.5 dB (HV) and ~~-25~~-25.0 dB (HH), since this was found to be a reasonable range of expected backscatter values. Figure 2 shows the image pair Fram Strait after the conversion into intensity values.

3.2 Sea ice drift algorithm

The presented sea ice drift algorithm is based on a combination of feature-tracking and pattern-matching, and is designed to utilise the respective advantages of the two approaches. Computationally efficient feature-tracking is used to derive a first estimate of the drift field. The provided vectors serve as initial search position for pattern-matching, that provides accurate drift vectors at each given location including rotation estimate and maximum ~~cross coefficient~~ cross-correlation value. As illustrated in the flowchart in Figure 3, the algorithm consists of five

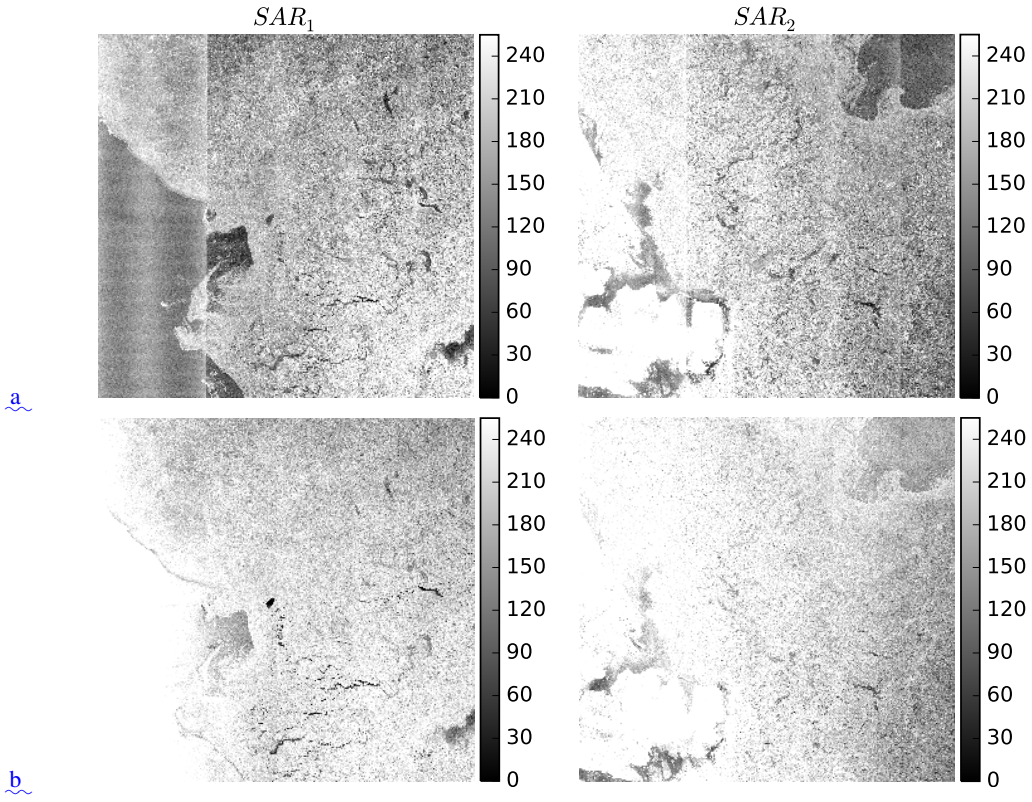

Figure 2. Image pair Fram Strait in (a) HV and (b) HH polarisation after conversion (Equation 2) from backscatter values σ^0 into intensity values with range $0 \leq i \leq 255$ using lower and upper brightness boundaries for HV: $\sigma^0_{\min} = -32.5\,\text{dB}$ and $\sigma^0_{\max} = -18.86\,\text{dB}$ and HH: $\sigma^0_{\min} = -25.0\,\text{dB}$, $\sigma^0_{\max} = -10.97\,\text{dB}$.

main steps: I Feature tracking, II Filter, III First guess, IV Pattern matching and V Final drift product.

I Feature-tracking

The feature-tracking algorithm used in this work is an adjusted version from Muckenhuber et al. (2016), who introduced a computationally efficient sea ice drift algorithm for Sentinel-1 based on the ORB (Oriented FAST and Rotated BRIEF) algorithm from Rublee et al. (2011). ORB uses the concept of the FAST keypoint detector (Rosten and Drummond, 2006) to find corners on several resolution levels. The patch around each corner is then described using an modified version of the binary BRIEF descriptor from Calonder et al. (2010). To ensure rotation invariance, the orientation of the patch is calculated using the intensity-weighted centroid. Muckenhuber et al. (2016) applies a Brute Force matcher that compares each feature from the first image to all features in the second image. The comparison of two features is done using the Hamming distance, that represents the number of positions in which the two compared binary feature vectors differ from each other. The

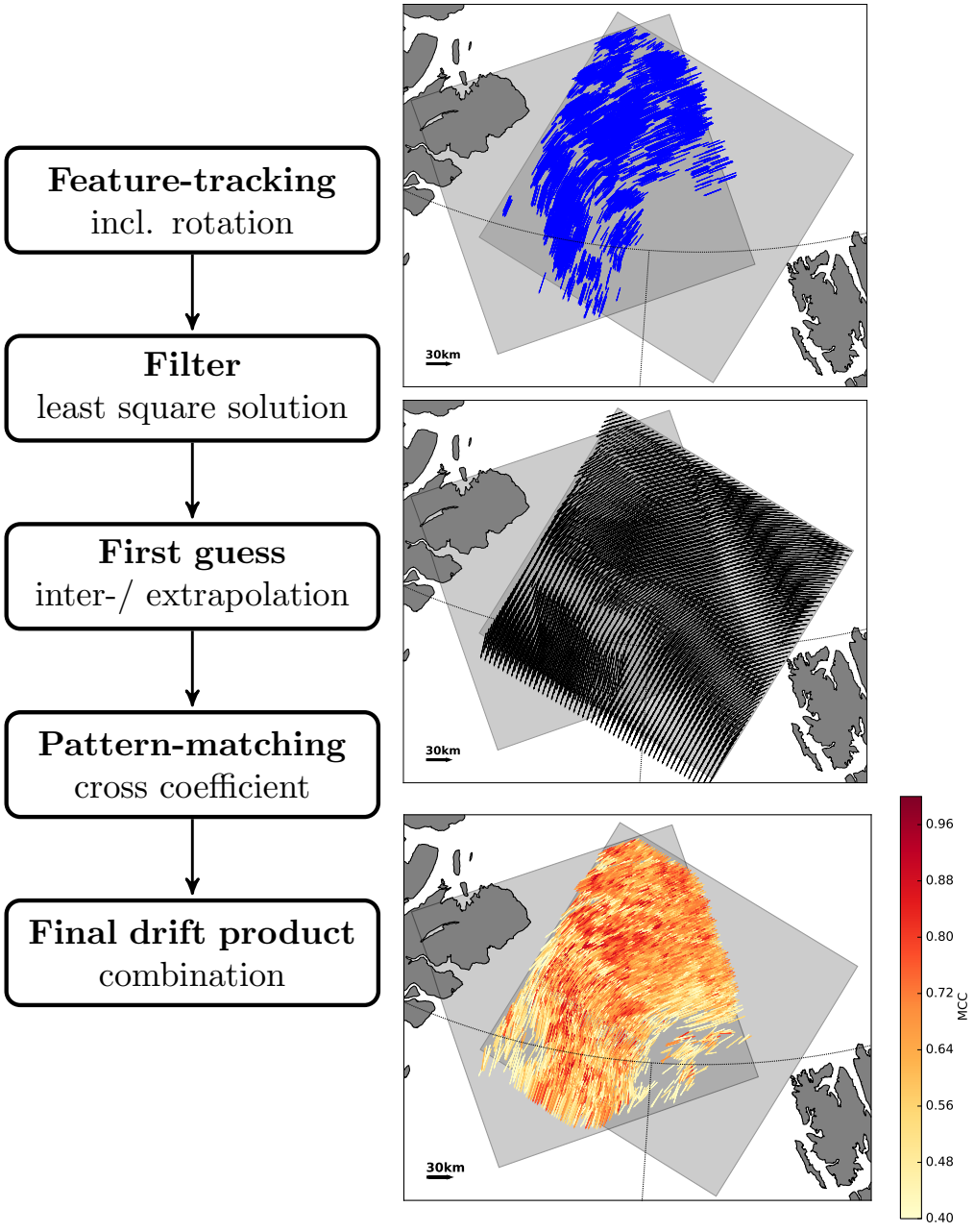

Figure 3. The flowchart on the left depicts the five main steps of the algorithm. The right column illustrates the evolution of the drift results using image pair Fram Strait in HV polarisation and a grid with 4 km spacing. Blue vectors are derived applying an adjusted version of the feature tracking algorithm from Muckenhuber et al. (2016). Black vectors indicate the initial drift estimate (first guess) based on filtered feature-tracking vectors. The final drift product (yellow to red vectors) are derived from combining the first guess with pattern-matching adjustment and applying a minimum ~~cross coefficient~~ cross-correlation value. In this example, a total of 4725 vectors have been found with a MCC value above 0.4 in 4 min.

best match is accepted if the ratio of the shortest and second shortest Hamming distances is below a certain threshold. Given a suitable threshold (and unique features), the ratio test will discard a high number of false matches, while eliminating only a few correct matches.

Muckenhuber et al. (2016) found ~~the most~~ a suitable parameter setting for our area and time period of interest, including a Hamming distance threshold of 0.75, a maximum drift filter of 0.5 $\mathrm{m/s}$, a patch size of 34×34 pixels and a resolution pyramid with 7 steps combined with a scaling factor of 1.2. Due to the resolution pyramid, the considered feature area varies from 2.7×2.7 km to 9.8×9.8 km and the resulting drift field represents a resolution mixture between these boundaries.

We adjust the algorithm from Muckenhuber et al. (2016) by applying a logarithmic scaling for the SAR backscatter values σ_0 instead of the previous used linear scaling (Section 3.1). In addition, we extract for each vector the rotation information α, i.e. how much the feature rotates from the first to the second image.

Applying the adjusted feature-tracking algorithm provides a number of un-evenly distributed vectors (e.g. blue vectors in Figure 3) with start positions x_{1f}, y_{1f} on the first image (SAR_1), end positions x_{2f}, y_{2f} on the subsequent image (SAR_2) and corresponding rotation values ~~α_f~~ $\alpha_{raw\,f}$. The index f represents a feature-tracking vector and ranges from 1 to F, with F being the total number of derived feature-tracking vectors.

To avoid zero-crossing issues during the following filter and inter-/extrapolation process (in case the image rotation δ between SAR_1 and SAR_2 is close to 0°), a factor $|180 - \delta|$ is added to the raw rotation values $\alpha_{raw\,f}$ using the following Equation:

$$\alpha_f = \begin{cases} \alpha_{raw\,f} + |180 - \delta| & \text{if } \alpha_{raw\,f} + |180 - \delta| < 360 \\ \alpha_{raw\,f} + |180 - \delta| - 360 & \text{if } \alpha_{raw\,f} + |180 - \delta| > 360 \end{cases} \tag{3}$$

This centres the reasonable rotation values in the proximity of 180°. After applying the filter and inter-/extrapolation process, the estimated rotation α is corrected by subtracting $|180 - \delta|$.

II Filter

To reduce the impact of potentially erroneous feature-tracking vectors on the following steps, outliers are filtered according to drift and rotation estimates derived from least squares solutions

using a third degree polynomial function. Considering a matrix **A**, that contains all end positions x_{2f}, y_{2f} in the following form

$$\mathbf{A} = \begin{pmatrix} 1 & x_{21} & y_{21} & x_{21}^2 & y_{21}^2 & x_{21} * y_{21} & x_{21}^3 & y_{21}^3 \\ 1 & x_{22} & y_{22} & x_{22}^2 & y_{22}^2 & x_{22} * y_{22} & x_{22}^3 & y_{22}^3 \\ \vdots & \vdots & \vdots & \vdots & \vdots & \vdots & \vdots & \vdots \\ 1 & x_{2F} & y_{2F} & x_{2F}^2 & y_{2F}^2 & x_{2F} * y_{2F} & x_{2F}^3 & y_{2F}^3 \end{pmatrix} \tag{4}$$

, we derive three vectors $\boldsymbol{b}_{x_1}$, $\boldsymbol{b}_{y_1}$ and $\boldsymbol{b}_{\alpha}$, that represent the least squares solutions for **A** and $\boldsymbol{x}_1 = (x_{11}, ..., x_{1F})$, $\boldsymbol{y}_1 = (y_{11}, ..., y_{1F})$ and $\alpha = (\alpha_1, ..., \alpha_F)$ respectively. The starting position x_{1f}, y_{1f} and the rotation α_f of each vector can then be simulated using a third degree polynomial function $f(x_{2f}, y_{2f}, \boldsymbol{b})$ depending on the end position x_{2f}, y_{2f} and the corresponding least squares solution $\boldsymbol{b} = (b_0, b_1, b_2, b_3, b_4, b_5, b_6, b_7)$.

$$f(x_{2f}, y_{2f}, \boldsymbol{b}) = b_0 + b_1 x_{2f} + b_2 y_{2f} + b_3 x_{2f}^2 + b_4 y_{2f}^2 + b_5 x_{2f} y_{2f} + b_6 x_{2f}^3 + b_7 y_{2f}^3 \tag{5}$$

If the simulated start position, derived from $f(x_{2f}, y_{2f}, \boldsymbol{b})$, deviates from the feature-tracking start position x_{1f}, y_{1f} by more than 100 pixels, the vector is deleted. The same accounts for rotation outliers. If the simulated rotation deviates from the feature-tracking rotation α_f by more than 60°, the vector is deleted. We found a third degree polynomial function to be a good compromise between allowing for small to medium scale displacement and rotation discontinuities, and excluding very unlikely vectors, that eventually would disturb the following steps. The parameters for the filter process, i.e. 100 pixels (displacement) and 60° (rotation), have been chosen according to visual interpretation using several representative image pairs. Figure 4 illustrates the filter process by depicting the results from image pair Fram Strait.

III First guess

The remaining feature-tracking vectors are used to estimate the drift incl. rotation on the entire first image, i.e. estimated x_2, y_2 and α values are provided for each pixel on SAR_1 (Figure 5). The quality of this 'first guess', however depends on the density of the feature-tracking vector field and the local ice conditions.

Between the feature-tracking vectors, estimated values are constructed by triangulating the input data and performing linear barycentric interpolation on each triangle. That means, the estimated values represent the weighted mean of the three neighbouring feature-tracking values. The interpolated value v_p at any pixel p inside the triangle is given by Equation 6, where v_1, v_2, v_3 represent the feature-tracking values at the corners of the triangle and A_1, A_2, A_3 are the areas of the triangle

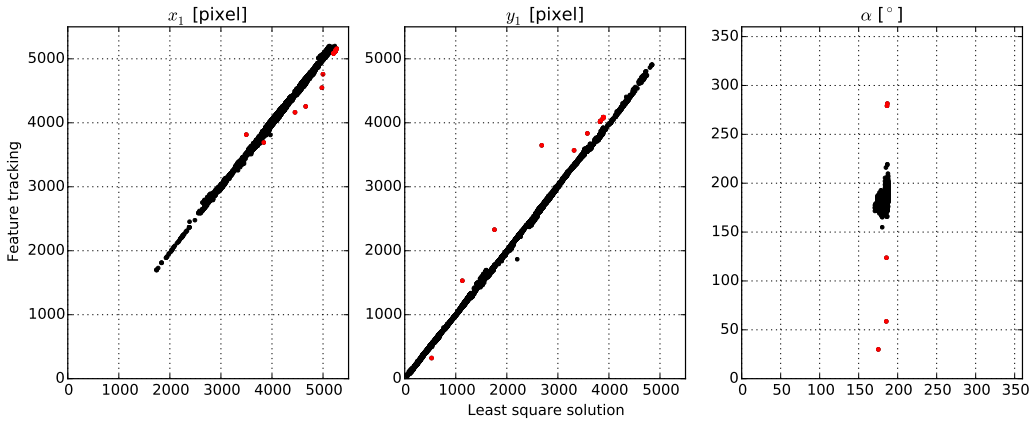

Figure 4. Filter process applied on image pair Fram Strait in HV polarisation. The x-axis represent the simulated start position and rotation, derived from $f(x_{2f}, y_{2f}, \boldsymbol{b})$ and the y-axis represent the feature-tracking start position x_{1f}, y_{1f} and rotation α_f. NB: the image rotation is $\delta = 129.08°$, which means the rotation was adjusted by 50.92° (Equation 3). Red points were identified as outliers and deleted.

constructed by p and the two opposite corners, e.g. A_1 is the area between p, and the corners with value v_2 and v_3.

$$v_p = \frac{A_1 v_1 + A_2 v_2 + A_3 v_3}{A_1 + A_2 + A_3} \tag{6}$$

To provide a first guess for the surrounding area, values are estimated based on the least squares solutions using a linear combination of x_1 and y_1. Considering a matrix $\mathbf{C}$, that contains all start positions x_{1f}, y_{1f} in the following form

$$\mathbf{C} = \begin{pmatrix} 1 & x_{11} & y_{11} \\ 1 & x_{12} & y_{12} \\ \vdots & \vdots & \\ 1 & x_{1F} & y_{1F} \end{pmatrix} \tag{7}$$

, we derive three vectors $\boldsymbol{d}_{x_2}$, $\boldsymbol{d}_{y_2}$ and $\boldsymbol{d}_{\alpha}$, that represent the least squares solutions for $\mathbf{C}$ and $\boldsymbol{x}_2 = (x_{21}, ..., x_{2F}), \boldsymbol{y}_2 = (y_{21}, ..., y_{2F})$ and $\alpha = (\alpha_1, ..., \alpha_F)$ respectively. The estimated end position x_2, y_2 and rotation α at any location can then be simulated using the linear function $f(x_1, y_1, \boldsymbol{c})$ depending on the start position x_1, y_1 and the corresponding least squares solution $\boldsymbol{d} = (d_0, d_1, d_2)$.

$$f(x_1, y_1, \boldsymbol{d}) = d_0 + d_1 x_1 + d_2 y_1 \tag{8}$$

As mentioned above, the rotation estimates α are now corrected for the adjustment applied in Equation 3, by subtracting $|180 - \delta|$.

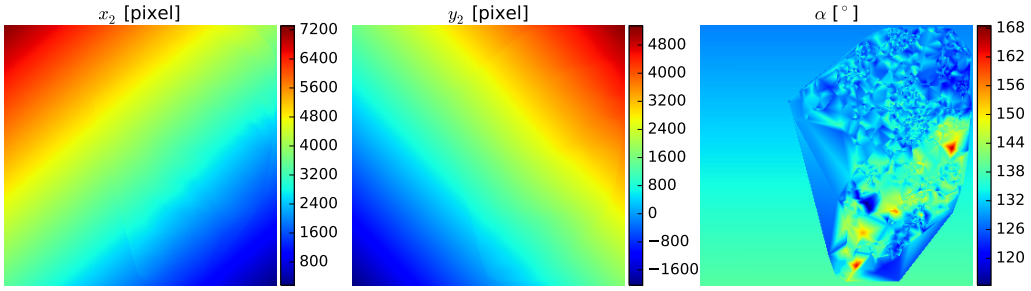

Figure 5. Example of estimated drift and rotation (first guess) based on filtered feature-tracking vectors using image pair Fram Strait in HV polarisation. The three panels show the components x_2, y_2 of the estimated end positions and the estimated rotation α for each pixel on the first image (SAR_1).

An example for the resulting first guess, i.e. estimated values for x_2, y_2 and α on SAR_1, is shown in Figure 5 and corresponding vectors are shown in black in Figure 3. Note that rotation α ~~includes~~ has already been corrected by subtracting $|180 - \delta|$. It includes now both the relative image rotation δ from SAR_1 to SAR_2 and the actual rotation of the feature itself. The introduced algorithm provides also the ~~relative image rotation~~ image rotation δ by projecting the left corners of SAR_2 onto SAR_1 and calculating the angle between the left edges of SAR_1 and SAR_2. The actual rotation of the features can easily be obtained by subtracting ~~the relative image rotation~~ δ from α.

IV Pattern-matching

The estimated drift field derived from feature-tracking provides values for x_2, y_2 and α at any location on SAR_1. The ~~uncertainty~~ representativeness of this estimate however, ~~increases with~~ depends on the distance d to the closest feature-tracking vector. Therefore, small to medium scale adjustments of the estimates are necessary, depending on the distance d. We apply pattern-matching at chosen points of interest to provide more accurate drift vectors and adjust the rotation estimate at these specific locations.

The used pattern-matching approach is based on the maximisation of the normalised ~~cross~~ cross-correlation coefficient. Considering a small template t_1 around the point of interest from SAR_1 with size $t_{1s} \times t_{1s}$ and a larger template t_2 around the location x_2, y_2 (defined by the corresponding first guess) from SAR_2 with size $t_{2s} \times t_{2s}$, the normalised ~~cross coefficient~~ cross-correlation matrix **NCC** is defined as (Hollands , 2012):

$$\mathbf{NCC}(x,y) = \frac{\sum_{x',y'}(t_1'(x',y')t_2'(x+x',y+y'))}{\sqrt{\sum_{x',y'} t_1'(x',y')^2 \sum_{x',y'} t_2'(x+x',y+y'))^2}} \tag{9}$$

$$t_1'(x',y') = t_1(x',y') - \frac{1}{t_{1s}^2} \sum_{x'',y''} t_1(x'',y'') \tag{10}$$

$$t_2'(x+x',y+y') = t_2(x+x',y+y') - \frac{1}{t_{1s}^2} \sum_{x'',y''} t_2(x+x'',y+y'') \tag{11}$$

with $t_1(x',y')$ and $t_2(x',y')$ representing the value of t_1 and t_2 at location x',y'. The summations are done over the size of the smaller template, i.e. x', y', x'' and y'' go from 1 to t_{1s}. Template t_1 is moved with step size 1 pixel over template t_2 both in horizontal (x) and vertical (y) direction and the ~~cross coefficient~~ cross-correlation values for each step are stored in the matrix **NCC** with size $(1+t_{s2}-t_{s1}) \times (1+t_{s2}-t_{s1})$. The highest value in the matrix **NCC**, i.e. the the maximum normalised ~~cross coefficient~~ cross-correlation value MCC, represents the location of the best match and the corresponding location adjustment is given by dx and dy.

$$(\frac{1+t_{s2}-t_{s1}}{2} + dx, \frac{1+t_{s2}-t_{s1}}{2} + dy) = \underset{x,y}{argmax}(\mathbf{NCC}(x,y)) \tag{12}$$

To restrict the search area t_{2s} to a circle, we set all values of **NCC** that are further than $t_{2s}/2$ away from the centre position to zero.

This limits the distance from the first guess to a constant value, rather than to an arbitrary value depending on the looking angle of the satellite. c To account for rotation adjustment, the matrix **NCC** is calculated several times: template t_1 is rotated around the initially estimated rotation α from $\alpha-\beta$ to $\alpha+\beta$ with step size $\Delta\beta$. The angle β is the maximum additional rotation and represents therefore the rotation restriction. The **NCC** matrix with the highest ~~cross coefficient~~ cross-correlation value MCC is returned.

To illustrate the pattern-matching process, an example, taken from image pair Fram Strait, is shown in Figure 6.

The described process demands the specification of four parameters: t_{1s}, t_{2s}, β and $\Delta\beta$.

The size of the small template $t_{1s} \times t_{1s}$ defines the considered area that is tracked from one image to the next and hence, affects the resolution of the resulting drift product. In order to be consistent with the resolution of the feature-tracking step and achieve our goal of a sea ice drift product with a spatial scaling of less than 5 km, we use the size of the feature-tracking patch of the pyramid level with the highest resolution to define the size of t_1. That means, we use $t_{s1} = 34$ pixels (2.7 km).

The size of the larger template $t_{2s} \times t_{2s}$ restricts the search area on SAR_2, i.e. how much the first guess can be adjusted geographically, and the angle β restricts the rotation adjustment of the first guess α. The three parameter t_{2s}, β and $\Delta\beta$ have a strong influence on the computational efficiency of the drift algorithm. Meaning that an increase of t_{2s}, β and a decrease of $\Delta\beta$ increase the

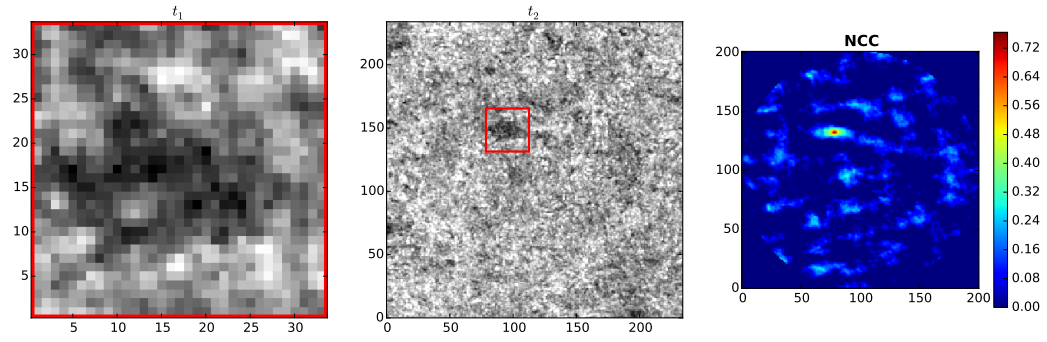

Figure 6. Pattern-matching using initial drift estimate from feature-tracking: The small template t_1 (left) around the point of interest on SAR_1 is rotated from $\alpha - \beta$ to $\alpha + \beta$ and matched with the large template t_2 (middle) from SAR_2, that has its centre at the estimated end position x_2, y_2. The right contour plot shows the normalised ~~cross coefficient~~ cross-correlation matrix **NCC** of the rotation β^* that provided the highest maximum ~~cross~~ cross-correlation coefficient MCC. The estimated end position x_2, y_2 of this example has to be adjusted by $dx = -21$ pixels, $dy = 32$ pixels to fit with the location of $MCC = 0.71$. Rotation adjustment β^* was found got be $3°$. NB: X and Y-axis represent pixel coordinates.

computational effort of the pattern-matching step. Based on visual interpretation of several repre-
365 sentative image pairs, we found $\Delta\beta = 3°$ to be a good compromise between matching performance and computational efficiency.

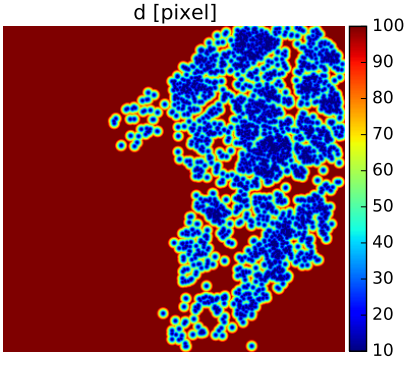

Figure 7. Example to illustrate the distribution of distance d to the closest feature-tracking vector using image pair Fram Strait in HV polarisation. Values outside the range $d_{min} \leq d \leq d_{max}$ are set to $d_{min} = 10$ and $d_{max} = 100$. The points with value d_{min} represent the start positions x_1, y_1 of the feature-tracking vectors on SAR_1.

Since the uncertainty of the first guess increases with distance d (Figure 7) to the closest feature-tracking vector, the search restrictions t_{2s} and β should increase with d. To find useful restrictions for t_{2s} and β, we calculated drift vectors using very high values for t_{2s} and β, i.e. being computationally

more demanding than we anticipate, and compared the results with the GPS drift buoy dataset from the N-ICE2015 expedition. Based on the results (Section 4) we found the following functions to represent useful restrictions for our area and time period of interest.

$$t_{2s}(d) = t_{1s} + 2d \qquad d_{min} \leq d \leq d_{max} \qquad d \in \mathbb{N} \tag{13}$$

$$\beta(d) = \begin{cases} 9 & \text{if } d < d_{max} \\ 12 & \text{if } d \geq d_{max} \end{cases} \tag{14}$$

The values for d_{min}, d_{max}, β and $\Delta\beta$ can easily be varied in the algorithm to adjust for e.g. different areas, drift conditions or a different compromise between matching performance and computational efficiency.

V Final drift product

In the last step, the small to medium scale displacement adjustments from pattern-matching are added to the estimated first guess derived from feature-tracking. Using buoy comparison, we found that the probability for large displacement errors decreases with increasing MCC value (Section 4). Therefore, vectors that have a MCC value below the threshold MCC_{min} are removed. We found $MCC_{min} = 0.4$ to be a good filter value, but this value can easily be adjusted in the algorithm depending on the sought compromise between amount of vectors and error probability. The algorithm returns the final drift vectors in longitude, latitude, the corresponding first guess rotation α and the rotation adjustment β in degrees and the maximum ~~cross coefficient~~ cross-correlation value MCC. An example for the final product is depicted with yellow to red coloured vectors in Figure 3. The colour scale refers to the MCC value, indicating the probability for an erroneous vector.

3.3 Comparison with buoy data

Sentinel-1 image pairs have been selected automatically according to position and timing of the GPS buoy data from the N-ICE2015 expedition. Each pair yielded more than 300 drift vectors ~~using~~ applying the feature-tracking algorithm from ~~Muckenhuber et al. (2016)~~ Section 3.2 and had a time difference between the two acquisitions of less than three days. Drift vectors have been calculated with the presented algorithm starting at the buoy GPS position with the least time difference to the acquisition of the first satellite image. The distance D between the calculated end position on the second image and the buoy GPS position with the least time difference to the second satellite acquisition has been calculated using the following equation:

$$D = \sqrt{(u - U)^2 + (v - V)^2} \tag{15}$$

where u and v represent eastward and northward drift components of the displacement vector derived by the algorithm, and U and V the corresponding drift components of the buoy.

4 Results

4.1 Search restrictions evaluation

To find suitable values for restricting the size of the search window t_{2s} and the rotation range defined by β, we calculated drift vectors, that can be compared to the considered GPS buoy dataset, using restrictions that are computationally more demanding than we anticipate for the recommended setting, i.e. $t_{2s} = 434$ pixels and $\beta = 18°$. These values corresponds to a possible pattern-matching adjustment of up to 200 pixels (16 km) and 18° in any direction independent of the distance d to the closest feature-tracking vector.

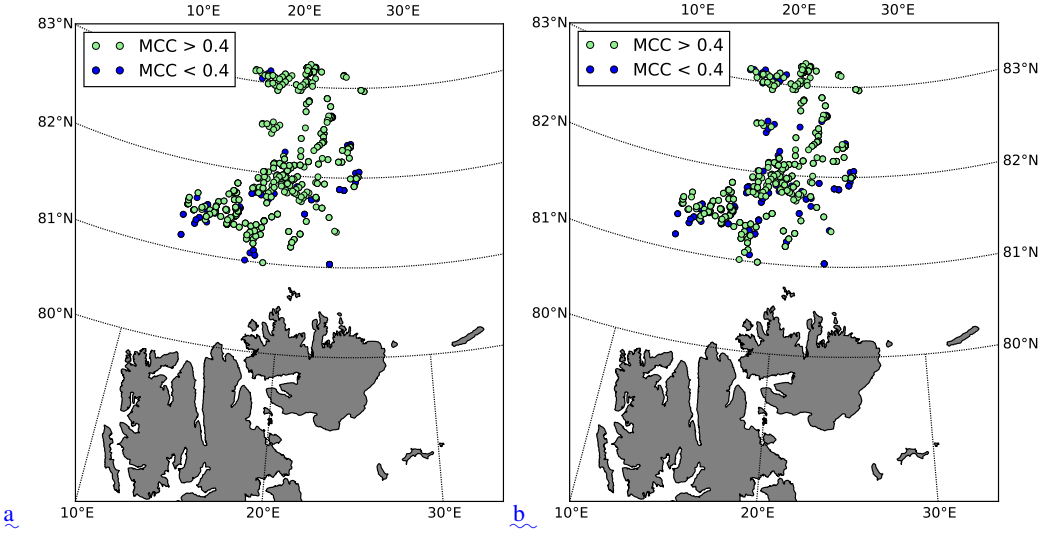

Figure 8. Considered buoy ~~trajectories~~ locations from the N-ICE2015 expedition that were used for comparison with algorithm results. Green and blue colour indicates start locations (on SAR_1) to which the algorithm provided vectors with a MCC value above and below 0.4 using (a) HV and (b) HH polarisation.

Based on an automatic search, we found ~~240~~ 244 matching Sentinel-1 image pairs (consisting of ~~110~~ 111 images), that allowed for comparison with ~~689~~ 711 buoy vectors (buoy locations are shown in Figure 8). The distance D (Equation 15) between the buoy location at the time of the second image SAR_2 and the corresponding algorithm result, represents the error estimate for one vector pair. To identify algorithm results that are more likely erroneous, vector pairs with a value D above 1000 m are marked with red dots in Figure 9 and Figure 10. Vector pairs with $D < 1000$ m are plotted with black dots.

Figure 9 and Figure 10 show the resulting pattern-matching adjustment of location (dx, dy) and rotation ($d\beta$) using the computationally demanding restrictions. The values are plotted against distance d to the next feature tracking vector in order to identify the dependence of the parameters on d. The blue lines in Figure 9 and Figure 10 indicate the recommended restrictions. This represents a compromise between computational efficiency and allowing the algorithm to adjust the first guess as much as needed for our time period and area of interest. The corresponding functions for $t_{2s}(d)$ and $\beta(d)$ are given in Equation 13 and Equation 14 and the recommended boundary values for distance d are $d_{min} = 10$ and $d_{max} = 100$.

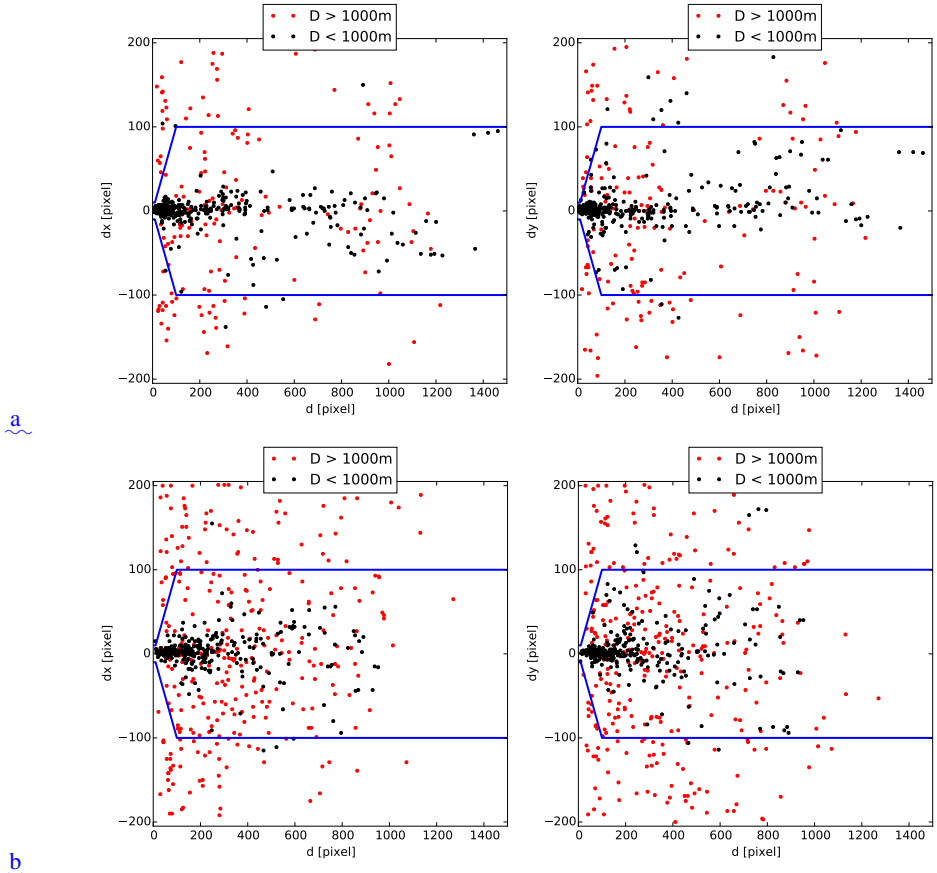

Figure 9. Pattern-matching location adjustment dx and dy in x and y direction versus distance d to closest feature tracking vector using (a) HV and (b) HH polarisation. D represents the difference between buoy GPS position and algorithm result. The blue lines indicate the recommended setting for t_{2s} (Equation 13) with $d_{min} = 10$ and $d_{max} = 100$.

4.2 Validation

Using the recommended search restrictions from above, the algorithm has been validated against the N-ICE2015 GPS buoy data set (Figure 8). The automatic search provided ~~241~~ 246 image pairs

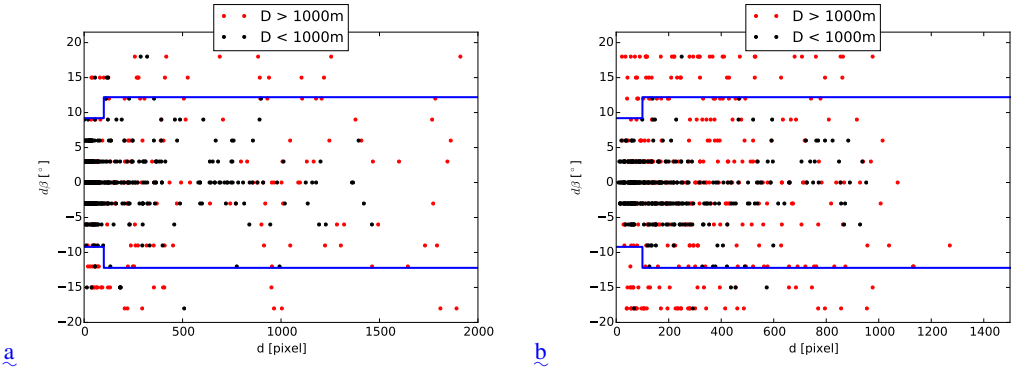

Figure 10. Pattern-matching rotation adjustment $d\beta$ versus distance d to closest feature tracking vector using (a) HV and (b) HH polarisation. D represents the difference between buoy GPS position and algorithm result. The blue lines indicate the recommended setting for β (Equation 14) with $d_{min} = 10$ and $d_{max} = 100$.

(consisting of ~~110~~ 111 images) and ~~714~~ 746 vectors for comparison for the considered time period (15th January to 22nd April) and area (80.5° N to 83.5° N and 12° E to 27° E). NB: this is a higher number of vectors than found for the evaluation of the search restrictions, since the used search windows t_2 are smaller and vectors closer to the SAR edge may be included.

The results of the conducted validation are shown in Figure 11. We found that the probability for a large D value (representative for the error) decreases with increasing maximum ~~cross coefficient~~ cross-correlation value MCC. Therefore we suggest to exclude matches with a MCC value below a certain threshold MCC_{min}. This option is embedded into the algorithm, but can easily be adjusted or turned off by setting $MCC_{min} = 0$. Based on the findings shown in Figure 11, we recommend a ~~cross~~ cross-correlation coefficient threshold $MCC_{min} = 0.4$ for our time period and area of interest. Using the suggested threshold reduces the number of vector pairs from ~~714 to 565.~~ 746 to 588 for the HV channel and to 478 for the HH channel.

The conducted validation also reveals a logarithmic normal distribution of the distance D (Equation 15) that can be expressed by the following probability density function (solid red line in Figure 11):

$$lnN(D;\mu,\sigma) = \frac{1}{\sigma D\sqrt{2\pi}} e^{-\frac{(\ln D-\mu)^2}{2\sigma^2}} \tag{16}$$

with μ and σ being the mean and standard deviation of the variable's natural logarithm. We found the mean and variance of the distribution lnN to be ~~$\mu = 5.835$ and $\sigma^2 = 1.584$. The median~~ $\mu = 5.866$ and $\sigma^2 = 1.602$ for HV polarisation and $\mu = 6.284$ and $\sigma^2 = 2.731$ for HH polarisation (solid red lines in Figure 11). The medians of the logarithmic normal distribution ~~is $e^{\mu} = 341.9\,m$~~ are $e^{\mu} = 352.9\,m$ for HV polarisation and $e^{\mu} = 535.7\,m$ for HH polarisation (dashed red ~~line~~ lines in Figure 11).

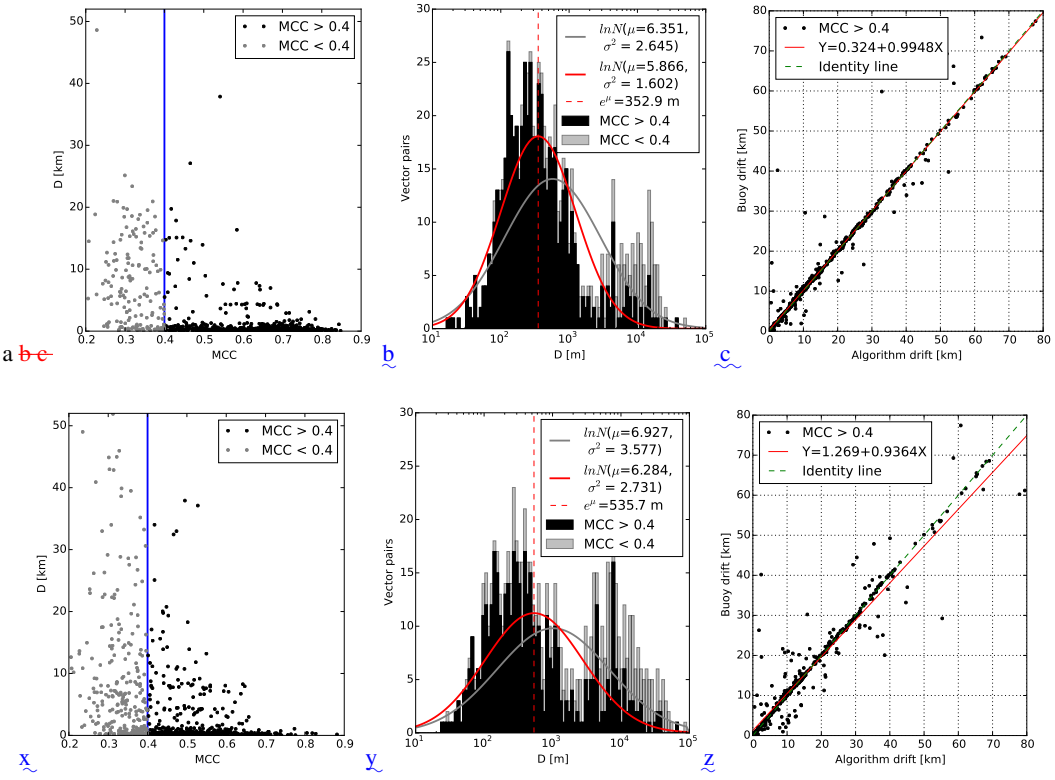

Figure 11. Calculated ice drift using recommended search restrictions compared to buoy GPS data using (a,b,c) HV and (x,y,z) HH polarisation. Light grey represents vectors with maximum ~~cross coefficient~~ cross-correlation values $MCC < 0.4$ and results after using the suggested threshold $MCC_{min} = 0.4$ are shown in black. (a,x) MCC values against distance D (Equation 15) between algorithm and buoy end position. The blue line indicates the recommended setting for $MCC_{min} = 0.4$. (b,y) Logarithmic histogram of distance D with 100 bins between 10 m and 10^5 m including ~~a~~ two logarithmic normal ~~distribution (solid red line)~~ distributions that ~~was~~ were fitted to all results (grey) and to the filtered results with $MCC > 0.4$ (solid red line). (c,z) Comparison of drift distance derived from algorithm against buoy displacement for the filtered results with $MCC > 0.4$.

4.3 Recommended parameter setting

Based on the restriction evaluation, our experience with the algorithm behaviour, and considering a good compromise between computational efficiency and high quality of the resulting vector field, we recommend the parameter setting shown in Table 1. The corresponding recommended values for $t_{2s}(d)$ and $\beta(d)$ are given in Equation 13 and Equation 14.

4.4 Computational efficiency

The processing time depends on the parameter setting and the chosen vector distribution. Using the recommended parameter setting from Table 1, allows high-resolution sea ice drift retrieval from

Table 1. Recommended parameter setting for sea ice drift retrieval from Sentinel-1 using the presented algorithm.

Parameter	Meaning	Recommended setting
$[\sigma^0_{\min}, \sigma^0_{\max}]$ (HH)	Brightness boundaries for HH channel	[-25 dB, -10.97 dB]
$[\sigma^0_{\min}, \sigma^0_{\max}]$ (HV)	Brightness boundaries for HV channel	[-32.5 dB, -18.86 dB]
t_{1s}	Size of template t_1	34 pixels (2.7 km)
$[d_{min}, d_{max}]$	Boundaries for distance d	[10 pixels, 100 pixels]
MCC_{min}	Threshold for ~~cross coefficient~~ cross-correlation	0.4
$\Delta\beta$	Rotation angle increment	3°

a Sentinel-1 image pair within a few minutes. Figure 3 depicts calculated ice drift vectors for the image pair Fram Strait on a grid with 4 km (50 pixels) spacing. The corresponding processing times are shown in Table 2. The calculations have been done using a MacBook Pro from early 2013 with a 2.7 GHz Intel Core i7 processor and 8 GB 1600 MHz DDR3 memory. The total processing time for 4725 vectors with a normalised ~~cross coefficient~~ cross-correlation value above 0.4, is about 4 minutes. This can be considered a representative value for an image pair with large overlap, good coverage with feature-tracking vectors and 4 km grid spacing.

The initial process in Table 2 'Create Nansat objects from Sentinel-1 image pair and read matrixes' takes the same amount of computational effort for all image pairs consisting of Sentinel-1 images with 400x400 km coverage.

The process 'I Feature-tracking' depends on the setting of the feature-tracking algorithm and varies strongly with the chosen number of features. Using the recommended setting from Muckenhuber et al. (2016), that includes the number of features to be 100000, the presented computational effort can be considered representative for all image pairs, independent of chosen points of interest and overlap of the SAR scenes.

The last process 'II Pattern-matching and III Combination' however, depends on the considered image pair and the chosen drift resolution. The computational effort is proportional to the number of chosen points of interest. Given a evenly distributed grid of points of interest, the computational effort increases with overlapping area of the SAR scenes, since pattern-matching adjustments are only calculated in the overlapping area. The effort potentially decreases with a higher number of well distributed feature-tracking vectors, since the size of the search windows t_2 (and slightly the range of the angle β) increases with distance d to the closest feature-tracking vector.

5 Discussion and outlook

To estimate the accuracy of the introduced algorithm, we compared drift results from ~~240~~ 246 Sentinel-1 image pairs with corresponding GPS positions from the N-ICE2015 buoy data set. We

Table 2. Processing time for sea ice drift retrieval from image pair Fram Strait on a grid with 4 km (50 pixels) spacing using HV polarisation (Figure 3). Representative for an image with large overlap and good coverage with feature-tracking vectors.

Process	Time [s]
Create Nansat objects from Sentinel-1 image pair and read matrixes	70
I Feature-tracking	66
II Pattern-matching and III Combination	107
$\sum$ Sea ice drift retrieval	243

found a logarithmic error distribution with a median at ~~341.9~~352.9 m for HV and 535.7 m for HH (Figure 11). The derived error values represent a combination of the following error sources:

- Timing: Buoy GPS data were collected every 1-3 hours and the timing does not necessarily match with the satellite acquisition time.
- Resolution: The algorithm returns the drift of a pattern (recommended size = 34 pixels, see Table 1), whereas the buoy measures the drift at a single location.
- Conditions: The ice conditions around the buoy is not known well enough to exclude the possibility that the buoy is floating in a lead. In this case, the buoy trajectory could represent a drift along the lead rather then the drift of the surrounding sea ice.
- actual error of the algorithm.

A main advantage of the combined algorithm compared to simple feature-tracking, is the user defined positioning of the drift vectors. The current algorithm setup allows the user to choose whether the drift vectors should be positioned at certain points of interest or on a regular grid with adjustable spacing. Constricting the pattern-matching process to the area of interest minimises the computational effort according to the individual needs.

The recommended parameters shown in Table 1 are not meant as a fixed setting, but should rather give a suggestion and guideline to estimate the expected results and the corresponding computational effort. The parameters can easily be varied in the algorithm setup and should be chosen according to availability of ~~time,~~ computational power, ~~number of image pairs, needed accuracy~~needed resolution, area of interest and expected ice conditions (e.g. strong rotation).

The presented combination of feature-tracking and pattern-matching can be applied to any other application that aims to derive displacement vectors computationally efficient from two consecutive images. The only restriction is that images need to depict edges, that can be recognised as keypoints

for the feature-tracking algorithm, and the conversion into intensity values i (Equation 2) needs to be adjusted according to the image type.

The remote sensing group at NERSC is currently developing a new pre-processing step to remove thermal noise on HV images over ocean and sea ice. First tests have shown a significant improvement of the sea ice drift results using this pre-processing step before applying the presented algorithm. This is ongoing work and will be included into a future version of the algorithm.

The European Space Agency is also in the process of improving their thermal noise removal for Sentinel-1 imagery. Noise removal in range direction is driven by a function that takes measured noise power into account. Until now, noise measurements are done at the start of each data acquisition, i.e. every 10-20 minutes, and a linear interpolation is performed to provide noise values every 3 seconds. The distribution of noise measurements showed a bimodal shape and it was recently discovered that lower values are related to noise over ocean while higher values are related to noise over land. This means, that Sentinel-1 is able to sense the difference of the earth surface brightness temperature similar to a passive radiometer. When the data acquisition includes a transition from ocean to land or vice versa, the linear interpolation fails to track the noise variation. The successors of Sentinel-1A/B are planned to include more frequent noise measurements. Until then, ESA wants to use the 8-10 echoes after the burst that are recorded while the transmitted pulse is still travelling and the instrument is measuring the noise. This will provide noise measurements every 0.9 seconds and allows to track the noise variations in more detail. In addition, ESA is planning to introduce a change in the data format during 2017 that shall remove the noise shaping in azimuth. These efforts are expected to improve the performance of the presented algorithm significantly (Personal Communication with Nuno Miranda, January 2017).

Having a computationally efficient algorithm with adjustable vector positioning allows not only to provide near-real time operational drift data, but also the investigation of sea ice drift over large areas and long time periods. Our next step is to embed the algorithm into a super-computing facility to further test the performance in different regions, time periods and ice conditions and evaluate and combine the results of different polarisation modes. The goal is to deliver large ice drift datasets and open-source operational sea ice drift products with a spatial resolution of less than 5 km.

This work is linked to the question how to combine the different timings of the individual image pairs in a most useful way. Having more frequent satellite acquisitions, as we get with the Sentinel-1 satellite constellation, enables to derive displacements for shorter time gaps and the calculated vectors will reveal more details e.g. rotational motion due to tides. As part of a scientific cruise with KV-Svalbard in July 2016, we deployed three GPS trackers on loose ice floes and pack-ice in Fram Strait. The trackers send their position every 5-30 min to deliver drift information with high temporal resolution. This efforts shall help to gain a better understanding of short-term drift variability and by comparison with calculated sea ice drift, we will investigate how displacement vectors from subsequent satellite images relate to sea ice displacements with higher temporal resolution.

The focus of this paper in terms of polarisation was put on the HV channel, since this polarisation provides on average four times more feature tracking vectors than HH and therefore delivers a finer initial drift for the first guess. We found our area of interest well covered with HV images, but other areas in the Arctic and Antarctic ~~reveal a better coverage~~ are currently only monitored in HH polarisation. Considering the four representative feature-tracking image pairs from Muckenhuber et al. (2016), the the relatively best HH polarisation performance (i.e. most vectors from HH, while at the same time fewest vectors from HV) was provided by the image pair that ~~showed~~ had the least time difference, i.e. 8 h, compared to 31 h, 33 h and 48 h. Therefore, we assume that the HV polarisation provides more features that are better preserved over time. And more consistent features ~~would~~ could also favour the performance of the pattern-matching step. ~~However,~~ Another argument is that the presented feature-tracking approach identifies and matches corners, which represent linear features. The linear features on HH images are more sensitive to changes in incidence angle, orbit and ice conditions than the linear features on HV images. This could explain the better feature-tracking performance of the HV channel. However, pattern-matching is less affected by changing linear features and more sensitive to areal pattern changes. This could potentially mean that the HH channel performs better than HV when it comes to pattern-matching. However, at this point, ~~this is just an assumption~~ these are just assumptions and will be addressed in more detail in our future work.

Utilising the advantage of dual polarisation (HH+HV) is certainly possible with the presented algorithm, but increases the computational effort. A simple approach is to combine the feature tracking vectors derived from HH and HV and produce a combined first-guess. Pattern-matching can be performed based on this combined first-guess for both HH and HV individually and the results can be compared and eventually merged into a single drift product. Having two drift estimates for the same position, from HH and HV pattern-matching respectively, would also allow to disregard vectors that disagree significantly. However, this option would increase the computational effort by two, meaning that the presented Fram Strait example would need about 8 min processing time.

After implementing the presented algorithm into a super-computing facility, we aim to test and compare the respective performance of HV, HH and HH+HV on large datasets to identify the respective advantages.

The current setting of the feature-tracking algorithm applies a maximum drift filter of 0.5 m/s. We found this to be a reasonable value for our time period and area of interest. However, when considering extreme drift situations in Fram Strait and a short time interval between image acquisitions, this threshold should be adjusted.

As mentioned above, we deployed three GPS tracker in Fram Strait and they recorded their positions with a temporal resolution of 5-30 min between 8^{th} July until 9^{th} September 2016 in an area covering 75° N to 80° N and 4° W to 14° W. Considering the displacements with 30 min interval, we found velocities above 0.5 m/s on a few occasions, when the tidal motion adds to an exceptionally fast ice drift.

The GPS data from the hovercraft expedition FRAM2014-2015 (https://sabvabaa.nersc.no), that was collected with a temporal resolution of 10 s between 31^{st} August 2014 until 6^{th} July 2015, did not reveal a single 30 min interval during which the hovercraft was moved by ice drift more than 0.45 m/s. The hovercraft expedition started at 280 km south from the North Pole towards the Siberian coast, crossed the Arctic Ocean towards Greenland and was picked up in the north-western part of Fram Strait.

In case the estimated drift from feature-tracking reaches velocities close to 0.5 m/s, the pattern-matching step might add an additional degree of freedom of up to 8 km, which could eventually lead to a higher drift result than 0.5 m/s, depending on the time interval between the acquisitions. The smaller the time difference, the larger is the potentially added velocity. In order to be consistent when combining the drift information from several image pairs with different timings, one should apply a maximum drift filter on the final drift product of the presented algorithm that has the same maximum velocity as the feature-tracking filter. The corresponding function is implemented in the distributed open-source algorithm.

Appendix A: Open-source distribution

The presented sea ice drift retrieval method is based on open-source satellite data and software to ensure free application and easy distribution. Sentinel-1 SAR images are distributed by ESA for free within a few hours of acquisition under https://scihub.esa.int/dhus/. The algorithm is programmed in Python (source code: https://www.python.org) and makes use of the open-source libraries Nansat, openCV and SciPy. Nansat is a ~~scientist friendly~~ Python toolbox for processing 2-D satellite Earth observation data (source code: https://github.com/nansencenter/nansat). OpenCV (Open Source Computer Vision) is a computer vision and machine learning software library and can be downloaded under http://opencv.org. SciPy (source code: https://www.scipy.org) is a Python-based ecosystem of software for mathematics, science, and engineering. The presented sea ice drift algorithm is distributed as open-source software under https://github.com/nansencenter/sea_ice_drift.

Acknowledgements. This research was supported by the Norwegian Research Council project IceMotion (High resolution sea-ice motion from Synthetic Aperture Radar using pattern tracking and Doppler shift, project number 239998/F50). We thank Polona Itkin and Gunnar Spreen for providing us the buoy GPS data that were collected as part of the N-ICE2015 project with support by the Norwegian Polar Institute's Centre for Ice, Climate and Ecosystems (ICE) and its partner institutes. The used satellite data were provided by the European Space Agency. We thank Nuno Miranda for information on ESA's de-noising efforts for Sentinel-1.

References

Berg, A. and Eriksson L.E.B.: Investigation of a Hybrid Algorithm for Sea Ice Drift Measurements Using Synthetic Aperture Radar Images IEEE Transactions on Geoscience and Remote Sensing, Vol. 52, No. 8, 5023–5033, 2014.

Calonder, M., Lepetit, V., Strecha, C., and Fua, P.: BRIEF: Binary Robust Independent Elementary Features, CVLab, EPFL, Lausanne, Switzerland, 2010.

ESA: Sentinel-1 ESA's Radar Observatory Mission for GMES Operational Services, ESA Communications, SP-1322/1, ISBN: 978-92-9221-418-0, ISSN: 0379-6566, 2012.

Hollands, T.: Motion tracking of sea ice with SAR satellite data, dissertaiton, Section 2: Estimation of motion from images, University Bremen, 2012.

Hollands, T. and Dierking, W.: Performance of a multiscale correlation algorithm for the estimation of sea-ice drift from SAR images: initial results, Ann. Glaciol., 52, 311–317, 2011.

IPCC – Intergovernmental Panel on Climate Change: Climate Change 2013: The Physical Science Basis, Fifth Assessment Report, AR5, 317–382, 323–335, 2013.

Komarov, A.S., and Barber, D.G.: Sea Ice Motion Tracking From Sequential Dual-Polarization RADARSAT-2 Images, IEEE Transactions on Geoscience and Remote Sensing, Vol. 52(1), No. 1, 121–136, doi: 10.1109/TGRS.2012.2236845, 2014.

Korosov A.A., Hansen W.M., Dagestad F.K., Yamakawa A., Vines A., Riechert A.: Nansat: a Scientist-Orientated Python Package for Geospatial Data Processing, Journal of Open Research Software, 4: e39, DOI: http:// dx.doi.org/10.5334/jors.120, 2016

Kwok, R., Curlander J.C., McConnell R., and Pang S.: An Ice Motion Tracking System at the Alaska SAR Facility, IEEE Journal of Oceanic Engineering, Vol. 15, No. 1, 44–54, 1990.

Muckenhuber S., Korosov A.A., and Sandven S. (2016): Open-source feature-tracking algorithm for sea ice drift retrieval from Sentinel-1 SAR imagery, The Cryosphere, 10, 913-925, doi:10.5194/tc-10-913-2016, 2016

Nansen, F.: The Oceanography of the North Polar Basin. Scientific Results, Vol. 3, 9, Longman Green and Co., Kristinania, Norway, 1902.

Pedersen, L.T., Saldo, R. and Fenger-Nielsen, R.: Sentinel-1 results: Sea ice operational monitoring, Geoscience and Remote Sensing Symposium (IGARSS), IEEE International, 2828–2831, doi=10.1109/IGARSS.2015.7326403, 2015

Rampal, P., Weiss, J., Marsan, D. and Bourgoin M.: Arctic sea ice velocity field: General circulation and turbulent-like fluctuations, Journal of Geophysical Research: Oceans, Vol. 114, Nr. C10014, doi=10.1029/2008JC005227, 2009.

Rampal, P., Weiss, J. and Marsan, D.: Positive trend in the mean speed and deformation rate of Arctic sea ice 1979–2007, Journal of Geophysical Research: Oceans, Vol. 114, Nr. C5013, doi=10.1029/2008JC005066, 2009b.

Rosten, E. and Drummond, T.: Machine learning for high-speed corner detection, in European Conference on Computer Vision, ISBN 978-3-540-33833-8, 430–443, doi: 10.100711744023_34, 2006.

Rublee, E., Rabaud, V., Konolige, K., and Bradski, G.: ORB: an efficient alternative to SIFT or SURF, IEEE I. Conf. Comp. Vis. (ICCV), ISBN: 978-1-4577-1101-5, 2564–2571, doi: 10.1109ICCV.2011.6126544, 6–13 Nov, 2011.

Spreen, G. and Itkin, P.: N-ICE2015 buoy data, Norwegian Polar Institute, https://data.npolar.no/dataset/6ed9a8ca-95b0-43be-bedf-8176bf56da80, 2015.

Thomas, M., Geiger, C. A., and Kambhamettu, C.: High resolution (400 m) motion characterization of sea ice using ERS-1 SAR imagery, Cold Reg. Sci. Technol., 52, 207–223, 2008.

Thorndike, A. S. and Colony, R.: Sea ice motion in response to geostrophic winds, Journal of Geophysical Research: Oceans, Vol. 87, Nr. C8, 5845–5852, doi=10.1029/JC087iC08p05845, 1982.

Widell, K., Østerhus, S. and Gammelsrød, T.: Sea ice velocity in the Fram Strait monitored by moored instruments, Geophysical Research Letters, Vol. 30, Nr. 19, doi=10.1029/2003GL018119, 2003.